European Journal of Medicinal Chemistry 246 (2023) 114909

Contents lists available at ScienceDirect

European Journal of Medicinal Chemistry

journal homepage: www.elsevier.com/locate/ejmech

Research paper

Novel thiazolidines of potential anti-proliferation properties against esophageal squamous cell carcinoma *via* ERK pathway

Marian N. Aziz [a,b], Linh Nguyen [c,d], Yan Chang [d,e], Delphine Gout [a], Zui Pan [d,e], Carl J. Lovely [a,*]

[a] Department of Chemistry and Biochemistry, 700 Planetarium Place, University of Texas at Arlington, TX, 76019, USA
[b] Department of Pesticide Chemistry, National Research Centre, Dokki, Giza, 12622, Egypt
[c] Dept. of Biology, College of Science, University of Texas at Arlington, TX, 76019, USA
[d] Department of Graduate Nursing, College of Nursing and Health Innovation, University of Texas at Arlington, TX, 76019, USA
[e] Bone and Muscle Research Center, University of Texas at Arlington, TX, 76019, USA

A B S T R A C T

The discovery of a new class of extracellular-signal-regulated kinase (ERK) inhibitors has been achieved via developing novel 2-imino-5-arylidene-thiazolidine analogues. A novel synthetic method employing a solid support-mediated reaction was used to construct the targeted thiazolidines through a cascade reaction with good yields. The chemical and physical stability of the new thiazolidine library has successfully been achieved by blocking the labile C5-position to aerobic oxidation. A cell viability study was performed using esophageal squamous cell carcinoma cell lines (KYSE-30 and KYSE-150) and non-tumorous esophageal epithelial cell lines (HET-1A and NES-G4T) through utilization of an MTT assay, revealing that (*Z*)-5-((*Z*)-4-bromobenzylidene)-*N*-(4-methoxy-2-nitrophenyl)-4,4-dimethylthiazolidin-2-imine (**6g**) was the best compound among the synthesized library in terms of selectivity. DAPI staining experiments were performed to visualize the morphological changes and to investigate the apoptotic activity. Moreover, western blots were used to probe the mechanism/pathway behind the observed activity/selectivity of thiazolidine **6g** which established selective inhibition of phosphorylation in the ERK pathway. Molecular modeling techniques have been utilized to confirm the observed activity. A molecular docking study revealed similar binding interactions between the synthesized thiazolidines and reported co-crystalized inhibitors with ERK proteins. Thus, the present study provides a starting point for the development of interesting bioactive 2-imino-5-arylidene-thiazolidines.

1. Introduction

Cancer is one of the most feared diseases worldwide due to its devastating impact on human health and its related death rate. Based on statistics from the International Agency for Research on Cancer (IARC), cancer incidence and mortality are growing rapidly. Thus, it is expected that the number of new cases will increase from 19.3 million in 2020 to 28.4 million in 2040 [1]. Tumor cells develop by deviation from the tightly controlled differentiation pathways of normal cells, through the loss or modification of normal regulatory growth mechanisms. There are over 200 different kinds of cancer that are usually classified based on the organ or cell where the tumor originated [2]. Thus, cancer is not a single disease but rather a collection which require individual treatment regimens. Tumor metastasis, which results in the spread of the primary tumor to secondary locations, is an additional complication, creating significant fear among patients. The metastasis process is mediated by a mechanism called “angiogenic-switch” in which a normal blood vessel becomes a dormant hyperplasia and then turns into a vascularized solid tumor acting as a lesion affecting surrounding organs [3]. Metastatic tumors are the real challenge in cancer treatment because a tumor cell in a specific organ may be converted into another tumor cell in other organs [4,5]. The complex mechanisms behind metastatic death-causing cancer are considered among the most important questions in cancer research [5,6]. Moreover, few of the approved drugs by the U.S. Food and Drug Administration (FDA) are targeted and effective against metastatic cancers [6]. Tumor cells can be characterized by their high death resistance, therefore searching for different approaches to induce cell death provides an intriguing approach to for the development of apoptotic drugs. Based on the morphological appearance of tumor cells, programmed cell death is categorized into three different types (apoptosis, autophagy, and necrosis).

Esophageal cancer, occurring in the upper gastrointestinal tract, is the 6th deadliest cancer with a total number of deaths numbering around 544,000 lives globally in 2020 [7]. It is one of the most common malignant neoplasms of the digestive tract and is characterized by high rate of incidence [8]. About 572,000 new cases were diagnosed as esophageal cancer worldwide in 2018; the number of cases increased to 604,000 by 2020 [9]. There are mainly two types of esophageal cancer:

* Corresponding author.
E-mail address: lovely@uta.edu (C.J. Lovely).

https://doi.org/10.1016/j.ejmech.2022.114909
Received 15 July 2022; Received in revised form 2 November 2022; Accepted 3 November 2022
Available online 24 November 2022

esophageal squamous cell carcinoma (ESCC) is the most common type worldwide, and esophageal adenocarcinoma is the predominant type in the USA, Australia, UK, and Western Europe [10,11]. The poor diagnosis and low survival rate (≤20%) of esophageal cancer are due to unclear/unnoticeable symptoms in the early stages of tumor development [12]. The gold standard approach for esophageal cancer treatment is radiotherapy, chemotherapy (using cisplatin and 5-fluorouracil), surgical resection, or their combination. Sadly, these approaches are not sufficient with many patients who suffer from advanced, inoperable, and metastatic diseases, especially when the cases are diagnosed at a late stage of the disease [13,14]. Recent studies show the importance of Ras/Raf/MEK/ERK pathway in esophageal carcinoma treatments and diagnosis especially for ESCC [15–19]. Therefore, our research group became interested in discovering and developing potent novel small molecules acting as ERK inhibitors. In the present study, we designed and synthesized novel small organic molecules based on the thiazolidine framework, then evaluated their anti-cancer activity in terms of induction of apoptosis and inhibition of ERK signaling pathway using in-*vitro* bioassays.

Mitogen-activated protein kinases (MAPK) are autophosphorylation protein kinases which react at serine and threonine residues to stimulate or deactivate their targets. MAPKs regulate essential physiological processes including proliferation, transformation, differentiation, apoptosis, stress response, and innate immunity [20–22]. There are three known kinase proteins belonging to the MAPK family, the extracellular signal-regulated protein kinases (ERK1/2), the p38 MAP kinases (α, β, δ, and γ), and the c-Jun NH2-terminal kinases ((JNK1/2/3)) [22,23]. ERK1/2 isoforms are dual-specificity kinases and are involved in the Ras-Raf-MEK-ERK signal transduction cascade. This cascade plays an important role in variety of cellular processes which are initiated by activation of RAS kinase, mediating the activation or phosphorylation of Raf-kinase and then MEK mediates the activation of ERKs. Ras mutations are common oncogenic alterations in many cancers and ultimately activate ERK1/2 pathway [20,21,24–27]. Therefore, discovering ERK inhibitors is a promising approach to cancer chemotherapy, indeed some ERK inhibitors are reaching clinical stages as potential anticancer agents. Fig. 1 shows some ERK inhibitors in clinical trials [28,29].

Apoptosis is recognized by the appearance of several morphological features, including cell rounding, shrinking of cytoplasm, condensed chromatin starting from the nuclear membrane to the whole nucleus, nuclear fragmentation, and generation of other organelles called apoptotic bodies [30–33]. There are number of intrinsic and extrinsic factors that activate the apoptotic process. Apoptotic ligands and/or drugs activate the extrinsic pathway by binding to death receptors of the tumor necrosis factor (TNF) receptor superfamily like Fas receptor (CD95), Death Receptor 4 and 5 (DR4 and 5) [24,34–36]. Thus, these ligands/drugs induce apoptosis by converting pro-caspases-8 and/or pro-caspases-10 into active forms of the death inducing signaling complex (DISC) [24]. Activation of caspase proteins is essential for the apoptotic process which cleave hundreds of proteins required for cellular functions, including nuclear and cytoskeletal proteins. Therefore, loss of these proteins causes plasma membrane changes and leads to shrinking in apoptotic cells [37]. However, apoptosis is an essential physiological process during development and aging stages, apoptotic anomalies are associated with a number of diseases including neurodegenerative, bacterial, viral, heart, autoimmune, and cancer [38–42].

The thiazolidine core structure is found in various synthetic compounds acting as anticancer agents [43–59], encouraging us to investigate novel thiazolidine derivatives. Moreover, thiazolidines show broad bioactivity against a global distribution of diseases such as inflammation [60–62], diabetic [63], fungal diseases [64], convulsant [65], parasites [66,67], HIV [68,69], and microbial diseases [70,71]. Thus, various synthetic methodologies have been developed for construction of the core thiazolidine ring structure. On-surface thiazolidine synthesis is one of the most efficient methods and environmentally favorable strategies reported to date. Our group has developed an on-silica gel-based technique for thiourea cyclization to produce thiazolidines in a one-pot reaction directly from propargyl amines and thioureas [72]. Scheme 1 outlines the sequential stages of developing our targeted novel thiazolidine compounds. The encouraging cytotoxicity results obtained for our first thiazolidine library led us to develop the present chemistry using the solid support technique as a green methodology towards constructing the thiazolidine scaffolds [73]. Most of the synthesized thiazolidines in the first library showed good antiproliferative activity against colon and breast cancer cell lines. Interestingly however, the several of synthesized thiazolidines were prone to oxidation by exposure to the atmospheric air resulting in the formation of the corresponding thiazolidinones **3** (Scheme 1a) [73].

In response therefore, a second library of thiazolidines was developed as a means to enhance their chemical and physical stabilities. The

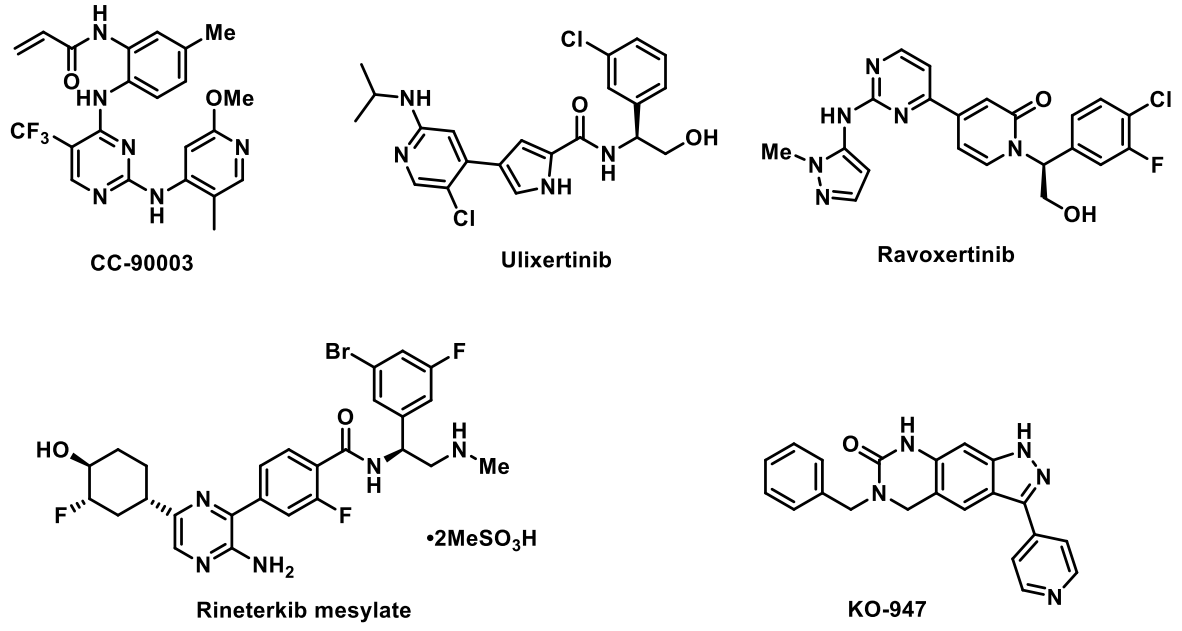

Fig. 1. ERK1/2 inhibitors in the clinical stages.

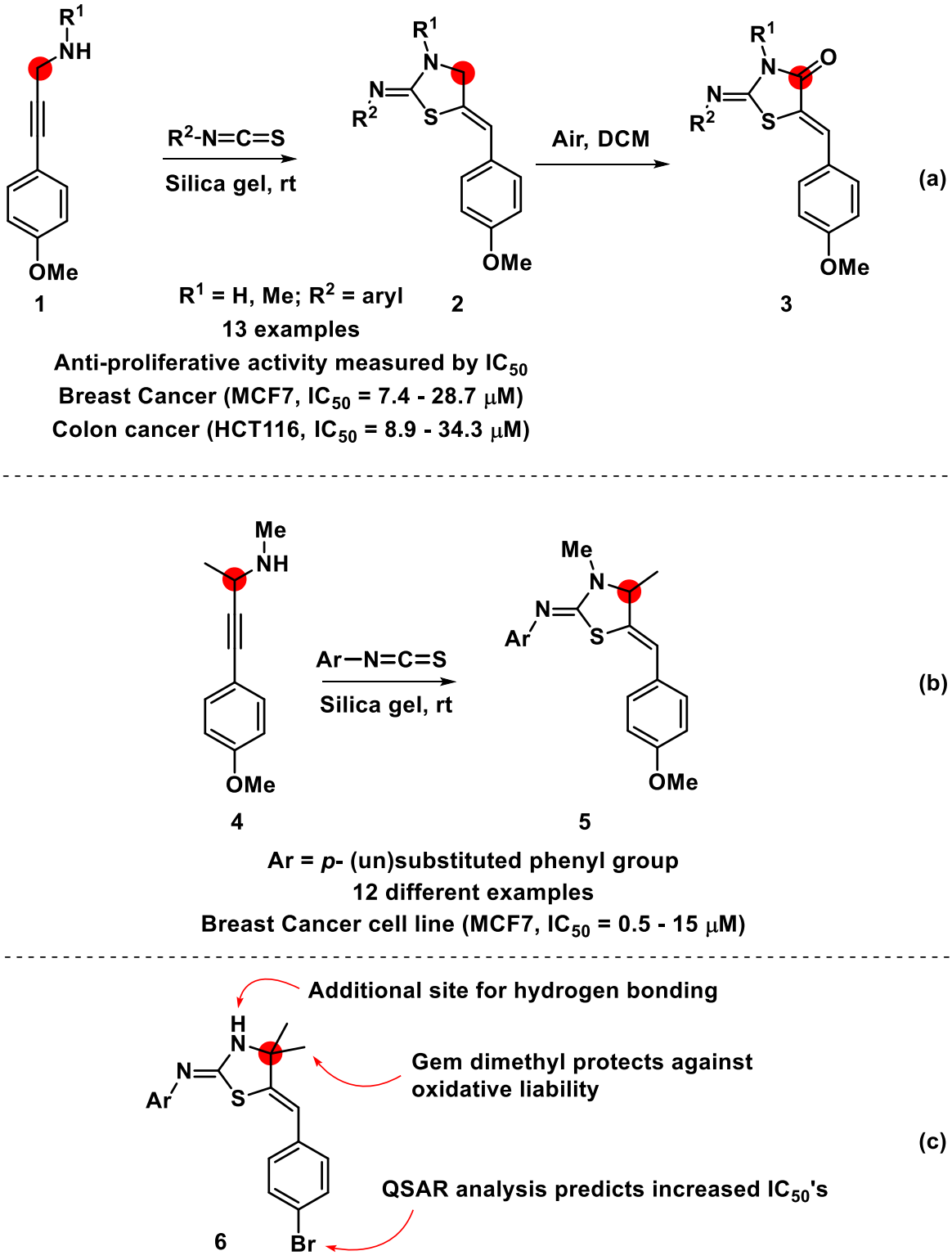

Scheme 1. (a) First generation anti-proliferative thiazolidines **2** and thiazolidones **3**. (b) Second generation anti-proliferative thiazolidines **5**. (c) Design of third generation thiazolidines (**6**).

core structure of thiazolidine ring was modified to block the oxidatively labile methylene group (CH_2) by introducing a methyl group to replace one hydrogen atom (Scheme 1b) but retaining the other functional groups within the core structure [74]. They revealed interesting anti-proliferative activity that was sufficiently encouraging to continue developing such chemistry toward synthesizing a stable and bio-active novel thiazolidines. However, unless the substituted thiazolidines **5** are protected from aerobic oxidation, they were still unstable at room temperature over the course of several days. Thus, another methyl group was introduced at that same position, so the two hydrogen atoms in the first library were now replaced with two methyl groups in the new series of thiazolidines (Scheme 1c). A second point, an initial thought was that

a *N*-methyl group in the core structure of thiazolidines as in the first two libraries (Scheme 1a and b) might cause strain within the ring and inductively activated the C5 position towards oxidation (stabilizing radical intermediates), thus affecting compound stability. Therefore, the *N*-methyl group was no longer incorporated, providing another potential site for binding *via* a hydrogen bond donor. Moreover, a qualitative structure activity relationship (QSAR) study has been performed based on the published data to predict the bioactivity of new thiazolidine derivatives using CODESSA-Pro (comprehensive descriptors for structural and statistical analysis) software [75]. The results show that replacing the methoxy group in the benzylidene ring with an electron withdrawing group should improve their corresponding IC_{50} values.

2. Results and discussion

2.1. Chemistry

The key propargyl amine 4-(4-bromophenyl)-2-methylbut-3-yn-2-amine (**9**) was synthesized via a Sonogashira cross-coupling reaction using 2-methylbut-3-yn-2-amine (**7**) , 1-bromo-4-iodobenzene (**8**) (to incorporate a halogenated group instead of methoxy group into benzylidene ring) in the presence of $PdCl_2(PPh_3)_2$ and CuI in a THF/TEA mixture (Scheme 2).[76] Then the synthesized propargyl amine **9** was mixed with isothiocyanate derivatives in the presence of silica gel as a solid support, resulting in isolation of the targeted thiazolidines. Initial experiments with this propargyl amine were conducted at room temperature as had been used previously, which resulted in consumption of the starting materials after two to three days (monitoring by TLC analysis). Presumably, the loss of the methyl groups compared to the previously reported systems reduces the reactive rotamer population thereby slowing down the reaction [73,77]. Therefore, the impact of elevating the temperature was investigated which resulted in identification of conditions leading to improved yields; ultimately finalized conditions consisted of stirring the slurry at 50–65 °C for 24 h. The isolated thiazolidines were purified by flash column chromatography, followed by crystallization using toluene or ethanol (Table 1). All the final products are stable crystalline solids at room temperature therefore one goal of this study, namely preparation of chemically and physically stable novel thiazolidines using our on-surface technique, has been achieved. All synthesized compounds were characterized using spectroscopic techniques (IR, ^{1}H NMR, ^{13}C NMR, HRMS) and a single crystal X-ray structure was obtained for one sample, compound 9 (see Scheme 2). Our initial expectation of removing the N-methyl group attached to thiazolidine-nitrogen (cf. **6** vs **2** or **5)** was releasing of some strain and potentially inversion of the geometry of exocyclic aryl imine group. However, on the basis of the X-ray study, it actually exhibits the same double bond geometry in the solid state as the two published libraries of thiazolidines and removing the *N*-methyl group does not affect the formation of (*Z*)-2-imino-(5*Z*)-ylidene thiazolidines.

Table 1
Synthesis of (*Z*)-5-((*Z*)-substituted benzylidene)-*N*-(4-bromophenyl)-4,4-dimethylthiazolidin-2-imine **6a-6i**.

Entry	Cpd.	Ar	Yield (%)[a]		IC_{50} (μM)
			I	II	
1	**6a**	4-BrC_6H_4	77	55	13.2
2	**6b**	4-ClC_6H_4	75	50	64.2
3	**6c**	4-FC_6H_4	77	46	10.6
4	**6d**	4-$NO_2C_6H_4$	95	30	31.5
5	**6e**	C_6H_5	80	54	18.6
6	**6f**	4-MeC_6H_4	78	34	64.3
7	**6g**	4-OMe-2-$NO_2C_6H_3$	94	44	16.8
8	**6h**	4-CH_3-3-ClC_6H_3	80	40	65.4
9	**6i**	4-$MeOC_6H_4$	85	42	14.2

[I] Isolated yields after chromatography purification.
[II] Isolated yields after crystallization.
[a] Reaction was performed with 1.0 mmol of 4-(4-bromophenyl)-2-methylbut-3-yn-2-amine and 1.0 mmol of the corresponding aryl isothiocyanate in a vigorous stirred silica gel (1.75 g) at 65 °C for 24 h.

2.2. Anti-cancer activity

2.2.1. Inhibitory effects of thiazolidine compounds on ESCC cells

The anti-cancer efficacy of the thiazolidine compounds in cultured human ESCC cell lines (KYSE-30 and KYSE-150) and esophageal non-tumorous epithelial cell lines (HET-1A and NES-G4T) were assessed using the gold standard MTT assay (3-(4,5-dimethylthiazol-2-yl)-2,5-diphenyl-2H-tetrazolium bromide) [78]. The activity of the thiazolidines was measured initially as IC_{50} values using eight different concentrations by incubation with KYSE-30 cells for 72 h, using RP4010 as a positive control [79]. The results of these experiments are shown in Fig. 2 (IC_{50} values for all the synthesized compounds against KYSE-30 cell line). For investigating the structure activity relationship (SAR) study, the thiazolidine structures were designed to have a variety of functional groups attached to exocyclic aryl amine such as electron withdrawing groups ((Br, Cl, F, NO_2), **6a-d** respectively),

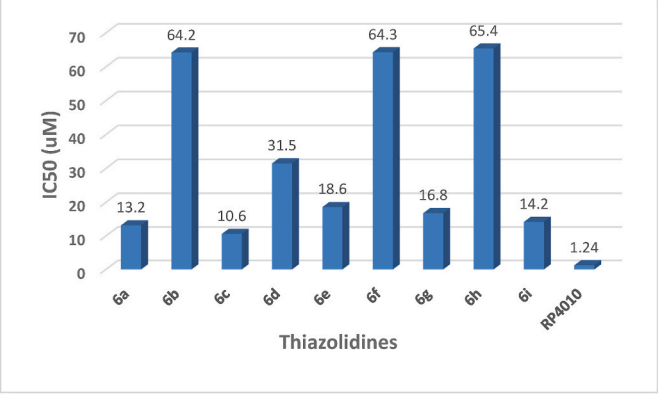

Fig. 2. IC_{50} values of thiazolidines **6a-i** tested with KYSE-30 cell line.

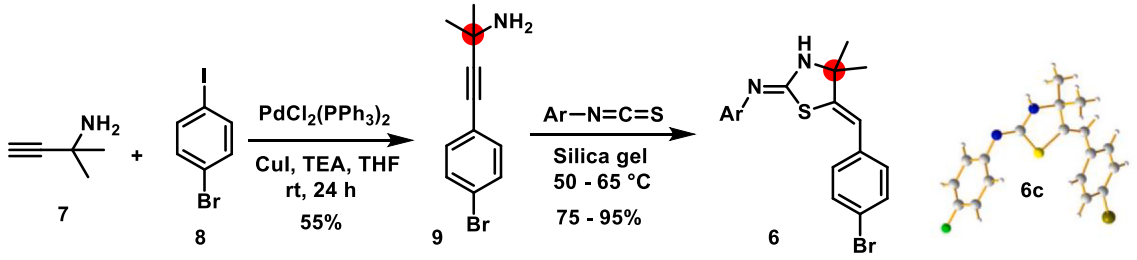

Scheme 2. Novel synthetized thiazolidines **6a-i** using on-surface methodology.

electron-donating groups (Me (**6f**), OMe (**6i**)), and bearing the two groups together as in compounds **6g** and **6h**. Comparing these derivatives with thiazolidine containing unsubstituted phenyl **6e** helps understanding the SAR of the synthesized compounds. All the derivatives reveal good inhibitory activity except ones containing Cl (**6b**), Me (**6f**) groups and combinations of both (**6h**). However, with the exception of thiazolidines containing Cl group, the data are consistent with the previously published data obtained for the two previously reported thiazolidine series [73,74]. Thiazolidines **6c**, **6a** and **6i** appear to be the most effective derivatives based on these initial data (10.6, 13.2, and 14.2 μM, respectively) compared to the unsubstituted exocyclic aryl amine **6d**. Interestingly, thiazolidines containing a methyl substituent group on the exocyclic aryl amine show a good inhibitory effect (14.2 μM) and the combination of methyl and nitro group on the exocyclic aryl amine **6g** retains the activity to be 16.8 μM. It was noticeable that the IC_{50} values of most of the effective compounds are close to 15 μM and for the less effective ones are higher than 60 μM. Therefore, the inhibitory effects for each compound using a single dose of 10 μM concentration for 72 h was assessed using two ESCC cell lines (KYSE-30 and KYSE-150) and HET-1A cells (Fig. 3). A general theme among all the tested compounds is the higher efficacy against KYSE-150 compared to HET-1A. However, modest selectivity of thiazolidines towards tumorous and non-tumorous cell lines was observed, compounds **6e** and **6g** reveal the lowest toxicity toward HET-1A cells. Therefore, a cell viability study of **6e** and **6g** with KYSE-30 and KYSE-150 was conducted using eight different concentrations (Fig. 4A). Compound **6g** displayed the highest efficacy against KYSE-150 cell line (71% inhibition of cell growth using 10 μM) among all the compounds. Also, the IC_{50} values support the choice of **6g** for further evaluation revealing inhibition of the proliferation of KYSE-30 and KYSE-150 using 16.8 μM and 10.07 μM, respectively. The IC_{50} of **6g** for HET-1A and NES-G4T were calculated as 13 μM and 202.2 μM, respectively. In general, the viability of all cell lines reduced in a dose-dependent manner during treatment of compound **6g** for 72 h as it is shown in Fig. 4B. Data suggest that **6g** could selectively inhibit cancer cell growth, while normal cells remained relatively insensitive, hence **6g** was selected for further analysis.

2.2.2. *Apoptosis analysis of 6 g in KYSE-30 and KYSE-150 cells*

4′,6-Diamidino-2-phenylindole dihydrochloride hydrate (DAPI) is a fluorescent sensitive staining dye that is useful for analyzing and visualizing nuclear changes and identifying cases of apoptosis. DAPI binds efficiently to adenine-thymine regions rich grooves in DNA. Using laser scanning confocal microscope with excitation and emission wavelength at 405 nm and 461 nm, respectively, DAPI fluorescence images can reveal the nuclear morphology of apoptotic cells such as chromatin fragmentation and condensation [80,81]. Therefore, nuclei staining of the cells treated with compound **6g** and stained with DAPI provided images that were obtained at various time points. As shown in Fig. 5, condensation of chromatin and fragmentation of nuclei membrane in both KYSE-30 and KYSE-150 when treated with **6g** at 10 μM were noticeable at 48 h and 72 h compared to the control. After 72 h, loss of nuclei integrity was apparent. This result reveals that **6g** could induce cell apoptosis.

2.2.3. *Compound 6g induced apoptosis through the ERK pathway*

Since ERKs and protein kinase B (Akt) play a key role in a number of cellular processes such as proliferation, transcription and apoptosis, they are being targeting for developing novel inhibitors of cancer growth [24, 82,83]. The potential mechanism of action of **6g** was examined *via* detecting expression of ERK and Akt proteins and their phosphorylated proteins by performing western blots on lysates of KYSE-150 and NES-G4T after treatment with 10 μL of compound **6g** after 4 h, 8 h, and 12 h.

For KYSE-150, Fig. 6A shows that **6g** down regulates pERK in a time dependent manner, while expression of Akt and pAkt seems similar from time zero till 12 h, compared to β-actin levels. Therefore, the ratio of pERK/ERK and pAkt/Akt were calculated and Fig. 6B shows a significant difference in the ratio pERK/ERK between 4 h and 12 h. Meanwhile, the pAkt/Akt ratio difference was insignificant as exposure duration increased. For NES-G4T, both pERK/ERK and pAKT/AKT ratio differences between 4 h and 12 h were not significant. These data demonstrate that treatment with **6g** induced apoptosis in ESSC cells through the ERK pathway but did not result in death of normal epithelial cells.

2.2.4. *Molecular modeling studies*

Molecular modeling techniques are helpful approaches in medicinal chemistry assisting in identification of the parameters behind biological properties [66]. Computer-aided drug discovery (CADD) can be classified based on the targeted biological receptor whether it is known/isolated or unknown, therefore, it is categorized as structure- and ligand-based techniques [84]. Molecular docking is the most common approach for ligand-based technique, while pharmacophore and quantitative structure-activity relationship techniques are used for the unknown targets and based on previously reported studies [84,85]. Thus, drug design (CADD) approaches play a vital role in the pharmaceutical search to accelerate the process of discovering new lead compounds. Using computational tools to analyze the actual facts and forming theoretical data helps in predicting the bioactivity of the designed

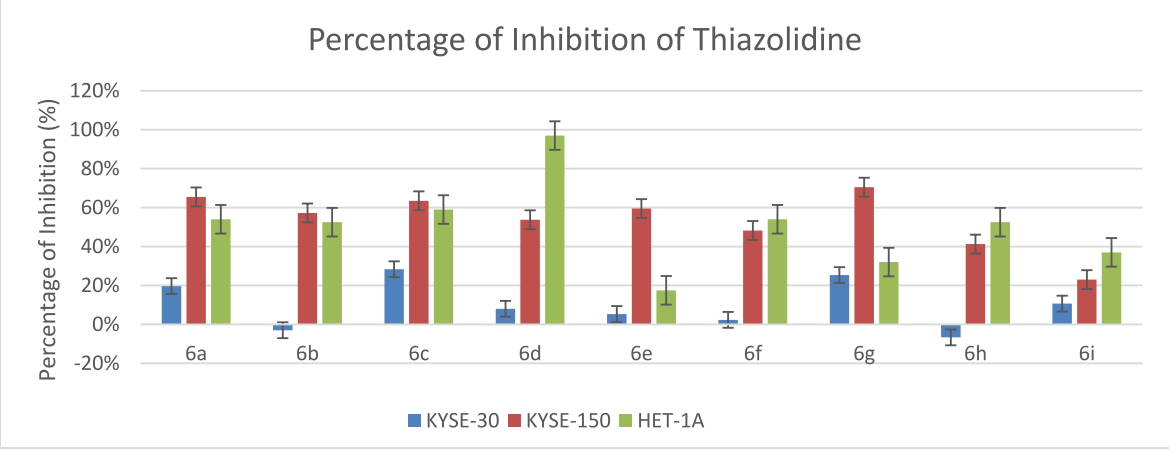

Fig. 3. Inhibitory effects on cell proliferation by thiazolidine compounds variations. Cell viability with thiazolidine compounds at 10 μM treatments for 72 h were calculated by MTT assay and normalized inhibitory effects were compared in KYSE-30, KYSE-150, HET-1A cells. Data were from 4 independent experiments with biological triplicates for each experiment.

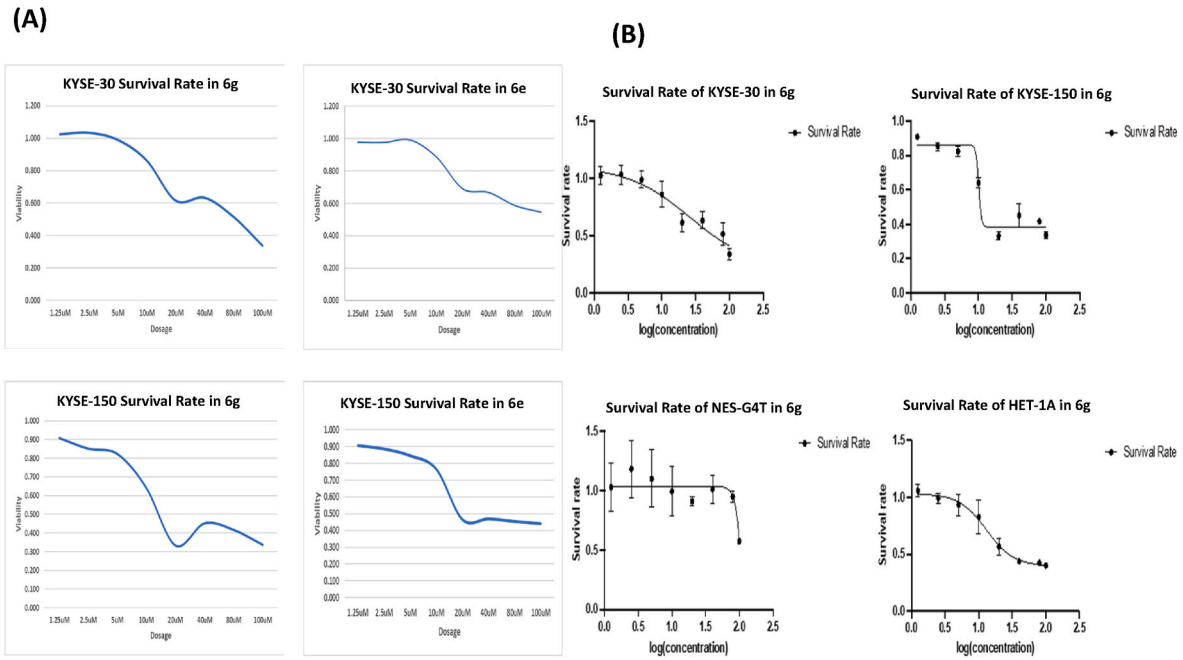

Fig. 4. Compound **6g** selectively inhibited cell proliferation in ESCC cells: (A) Cell viability of KYSE-30 and KYSE-150 with **6e** and **6g** compounds at eight different concentrations using MTT assay; (B) Cell viability with **6g** treatment after 72 h were calculated by MTT assay in KYSE-30, KYSE-150, HET-1A, and NES-G4T.

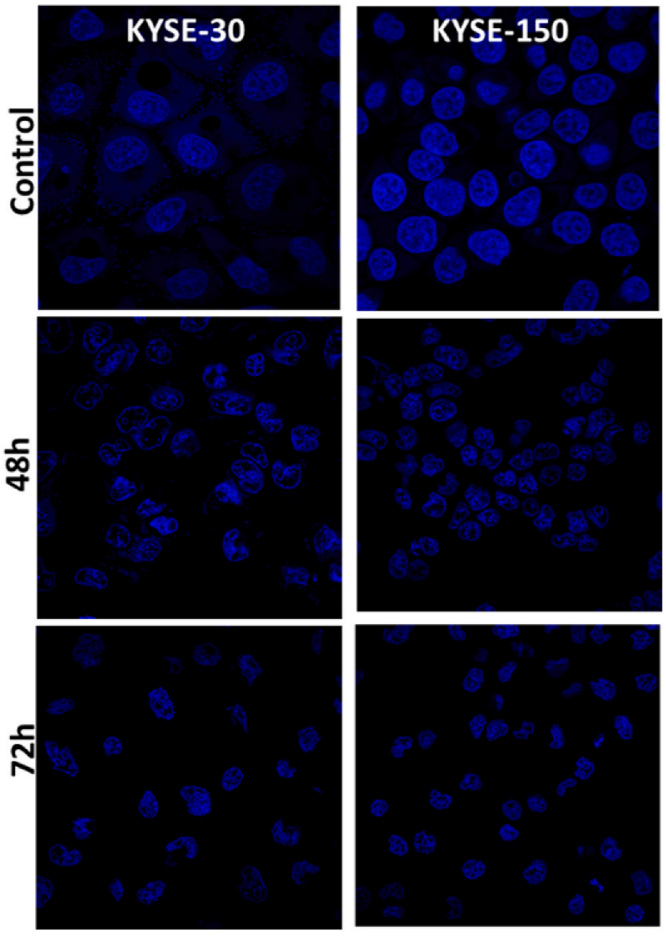

Fig. 5. DAPI staining of KYSE-30 and KYSE-150 cells treated with **6g** for 48 h, and 72 h.

molecules. It also provides rational ideas that help in modification and developing new novel compounds.

2.2.4.1. Molecular docking study. Molecular docking is a helpful tool in discovering novel candidates with improved potency based on previously isolated and co-crystalized lead/drug compound with targeted protein. There are a number of ERK inhibitors which have been co-crystalized with ERK proteins (Figs. 1 and 7) and some of them have been moved into clinical trials [86–88].

Molecular docking techniques have been useful for designing the targeted thiazolidines, confirming the observed biological activity and helping improve the activity for future designed thiazolidines and other derivatives. From recent studies performed by pharmaceutical companies, it is obvious that the newly discovered ERK inhibitors bind to a number of amino acid residues in the target pocket with more hydrogen bond interactions thus improved and confirmed the corresponding activity compared to ulixertinib [86,88]. For instance, the Astex and Sygnature compound reveals hydrogen bonds with MET108 and LYS114 which is different from the clinical candidate ulixertinib. Similar observations have been made while running the standard CDOCKER technique (Discovery Studio 2.5 software, Accelrys Inc., San Diego, CA, USA) for our synthesized thiazolidines. Ulixertinib exhibits three hydrogen bond interactions due to the terminal alcohol moiety with LYS54 and ASP167, π-cation and π-σ interactions between *p*-chlorophenyl and LYS54 with docking score −56.4471 kcal/mol. The thiazolidine docking studies show that the interactions with LYS54 are as expected and common among all the synthesized thiazolidine derivatives whether through hydrogen bond or π-cation interactions. Electron withdrawing groups attached to the aniline moiety makes the Br group attached to the benzylidene ring interact with LYS54 via a hydrogen bond interaction (**6a-b/g-h**) or π-cation interactions (**6c-d**). Derivatives containing electron-rich groups attached to the aniline ring engages in π-cation interactions with LYS54 with phenyl ring of aniline moiety (**6e-f**). The synthesized thiazolidines exhibit hydrogen bond interactions via the free NH thiazolyl group except compounds **6a-d**. As it is shown from the previously published work that interaction with MET108 is one of the main interactions corresponding to the observed activity [88], similar observations were made with three of the

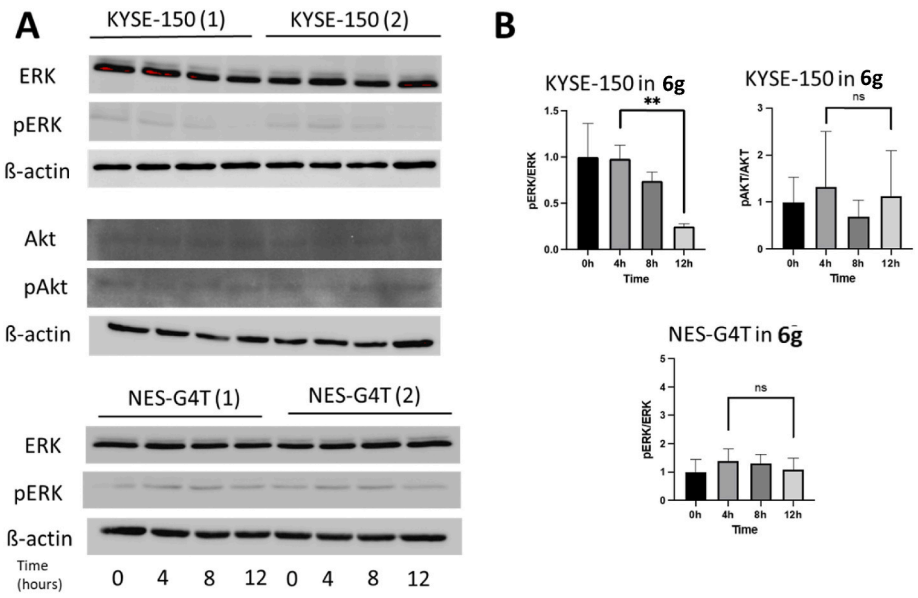

Fig. 6. Induced apoptosis through the ERK pathway in KYSE-150 cells. (A) Western blots of proteins ERK, pERK, Akt, and pAkt in KYSE-150 and NES-G4T treated with **6g** (10 μL) for 4 h, 8 h, and 12 h. Beta actin was used as the loading control. (B) Statistical data analysis of western blot results. Data is showed as mean ± SEM. $^{**}p \leq 0.05$.

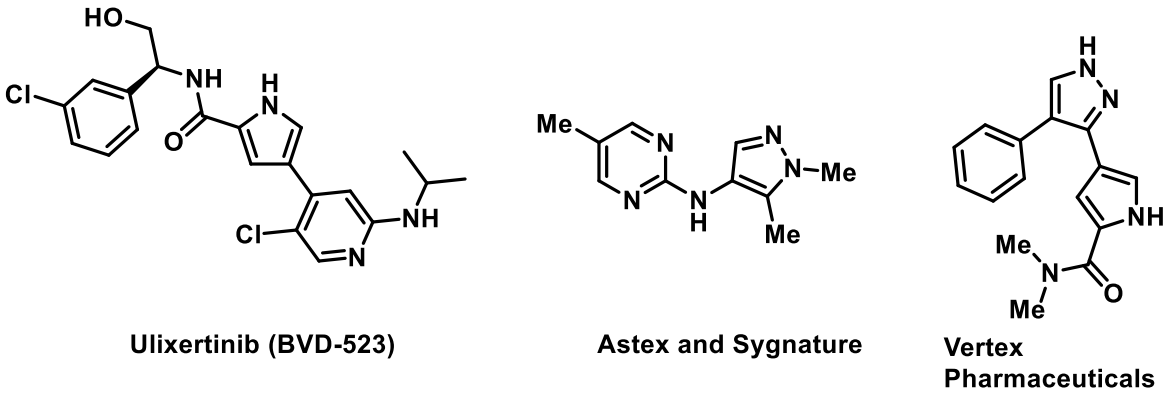

Fig. 7. Some important ERK inhibitors.

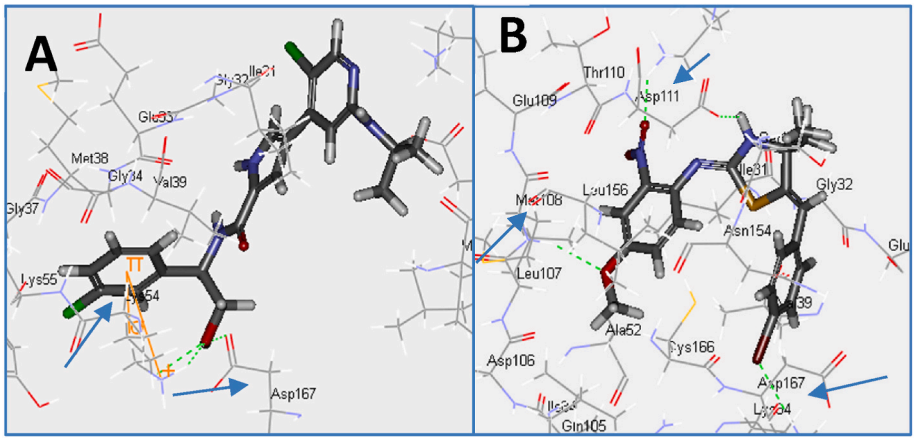

Fig. 8. The docking study of 6gdq ERK protein with ulixertinib (A) and an example of thiazolidines (6 g) (B).

synthesized thiazolidines (**6c-d** and **6g**) via the anilinyl moiety substituted with electron withdrawing groups. Among all the synthesized thiazolidines, compound **6g** exhibits the best docking score (the lowest binding energy) −47.5406 kcal/mol with the highest number of hydrogen bonds which supports its choice for further examination among all other synthesized compounds and is consistent with the observed biodata. Also, the second two best thiazolidines in terms of binding interactions are **6c** and **6d**, showing close docking scores −42.6524, and - 42.5816 kcal/mol, respectively. Thus, this docking study confirms that the binding interactions of our novel thiazolidines are consistent with the reported docking features of published and clinically valid ERK inhibitors. Moreover, all the previously mentioned observations support our initial design for this third thiazolidine library in which the electron deficient aryl rings were important for the expected activity based on the previous two studies of two thiazolidine libraries. To investigate the importance of the imino group, we removed the nitrogen from the exocyclic double bond and performed a docking study for all the compounds. Interestingly, only two common hydrogen bond interactions were noticed with ASP111 with thiazolyl NH and LYS54 with Br attached to benzylidene system (example of **6g** without imine nitrogen). Thus, the imino nitrogen was crucial for MET108 interactions as it is shown from Fig. 8B interactions of **6g** forming four different hydrogen bond interactions (thiazolyl NH – ASP111, NO_2 – LYS114, OMe – Met108, and Br – LYS54). Comparing compound **6g** with ulixertinib, thiazolidine **6g** exhibits more hydrogen bond interactions especially with MET108 which matches with other reported ERK inhibitors, and also, the docking scores for **6g** and ulixertinib are quite close in value. Details of the studies are included in the supporting information file.

2.2.4.2. 3D-pharmacophore study. Employing a 3D-pharmacophoric approach can illuminate the parameters governing bio-properties in terms of molecular structural elements/functions with chemical properties (hydrogen bonding, charge ionizable … etc.) in a 3D-array [67]. The synthesized thiazolidines **6a–i** were investigated using Discovery Studio 2.5 software following the standard protocol for assigning the 3D-pharmacophoric model [67]. Determination of the thiazolidinyl functional group interactions with the pharmacophoric features will assist in understanding the parameters necessary for bio-activity. Three pharmacophoric features (two hydrophobics "H-1, H-2" and a hydrogen-bonding acceptor) are the components of the 3D-array (Supplementary Table S1; Figs. S1 and S2).

All the tested compounds show alignment of the phenyl group and its bromine substituent attached to the thiazolindinyl C-5 with H-1 and H-2, respectively. The sulfur heteroatom of the thiazolidinyl heterocycle is aligned with the hydrogen-bonding feature. The latter observation can explain the effect of the (un)substituted phenyl linked through imino linkage to the C-2 of thiazolidinyl heterocycle in controlling the antiproliferative activities. The different fits of the pharmacophoric features led to variable estimated bio-properties. The estimated antiproliferative properties of the effective agents synthesized **6a**, **6c** and **6i** (IC_{50} = 17.6–19.0 μM) are consistent with their experimentally observed values (IC_{50} = 10.6–14.2 μM). The same for the weak antiproliferative agents discovered.

2.2.4.3. QSAR study. A mathematical equation obtained through QSAR techniques is capable of describing the biological properties in the form of physico-chemical/descriptor parameters which are the items necessary for interpretation the bio-observations. QSAR model of the synthesized thiazolidines **6a-i** was assigned by CODESSA-Pro software utilizing BMLR (best multi-linear regression) [68]. A two descriptor QSAR model was obtained with good correlation coefficient (R^2 = 0.852) (Supplementary Tables S2–S4, Fig. S3). Hydrogen bonding acceptor dependent HDCA-1/TMSA (MOPAC PC) (all) is a charge-related descriptor (t = −3.778). The appearance of this descriptor with its high coefficient value (−116.298) supports the observation due to the aforementioned 3D-pharmacophoric modeling technique revealing the alignment of hydrogen-bonding feature with the thiazolidinyl sulfur. The impact of this descriptor on the estimated antiproliferation properties is obvious due to its high coefficient value. This is easily revealed in compounds **6h** and **6i** which possess descriptor values = 0.01462, 0.01818 corresponding to estimated antiproliferative properties IC_{50} = 67.1, 11.2 μM, respectively. In other words, any minor differences in the descriptor value will greatly affect the estimated property due to high coefficient value of this descriptor. The molecular fractional hydrogen bonding donor ability can be calculated by equation (1) [69].

$$FHDCA1 = \frac{HDCA1}{TMSA} \tag{1}$$

Since, $HDCA1$ stands for to the hydrogen bonding donor ability of an atom. $TMSA$ is corresponding to total molecular surface area.

Minimum one-electron reactivity index for atom N is a semi-empirical descriptor with negative coefficient value (−84.6416). Thus, the high mathematical descriptor value of an agent observes high estimated antiproliferative compound and vice versa as revealed by compounds **6a** and **6b** that possess descriptor values 0.00455, −0.00421 corresponding to estimated properties IC_{50} = 12.8 and 60.4 μM, respectively. The Fukui atomic one-electron reactivity index can be determined by equation (2) [69].

$$R_A = \sum_{i\in A}\sum_{j\in A} C_{iHOMO}C_{jLUMO} \Big/ (\varepsilon_{LUMO} - \varepsilon_{HOMO}) \tag{2}$$

Since, C_{iHOMO} and C_{jLUMO} stand for the highest occupied and the lowest unoccupied molecular orbital coefficients. The ε_{LUMO} and ε_{HOMO} stand for the lowest unoccupied and the highest occupied molecular orbital energies.

Statistical internal validation parameters including standard deviation (s^2 = 0.021) and Fisher criteria (F = 17.300) support the goodness of the optimized QSAR model. The comparative cross-validation values of leave-one-out (R^2cvOO = 0.729) and leave-many-out (R^2cvMO = 0.783) to that of the QSAR equation (R^2 = 0.852) also add support to the robust nature of the model. Additionally, the correlation due to the estimated and experimental observed antiproliferation properties of the tested thiazolidines preserving their potencies among each other is also a good sign for the success of the QSAR model. To conclude, the molecular modeling investigation provides a QSAR model confirming the observed features analyzed by the pharmacophore technique, revealing the importance of the sulfur atom in the core structure of our designed and synthesized compounds. Moreover, the existence of an electron deficient aryl system attached to the thiazoldinyl core motif is crucial for the expected activity and that supports the observed experimental values, in addition to the importance of the imine nitrogen (docking model). Thus, based on these data generated from this novel class of ERK inhibitors, further improvements will be explored in the near future based on the current molecular modeling techniques.

3. Conclusion

In summary, a novel class of 2-imino-5-arylidene-thiazolidines has been discovered using an environmentally benign methodology. Discovery of stable thiazolidines has emerged through three stages by synthesizing three libraries of the targeted 2-imino-5-arylidene-thiazolidines via the chemistry developed in the Lovely lab. The reported library achieves the best chemical and physical stabilities to date and establishes a new class of bioactive thiazolidines. The antiproliferative activity of the synthesized thiazolidines was tested using two different ESCC cell lines, KYSE-30, KYSE-150 and two non-tumorigenic epithelial cell lines, HET-1A, and NSE-G4T cells. The MTT assay was performed to study the cell viability under treatment with 10 μM of synthesized

thiazolidines, revealing two compounds (**6e** and **6g**) out of the nine synthesized thiazolidines are the best ones among the group. Further cell viability studies of eight different concentrations of the two compounds were performed for selecting the most toxic compound against carcinomic cell line and least effective against non-tumorigenic cell lines, resulting in selection of **6g** for further investigations. DAPI staining was utilized to investigate the morphological changes as a result of cytotoxicity of **6g** against carcinomic KYSE-30 and KYSE-150 cell lines. The microscopic imaging guided us in selecting the KYSE-150 cell line which expresses antiapoptotic effect on the cell morphology. Therefore, two kinases (ERK and AKT) were targeted to be tested with thiazolidine **6g** using qRT-PCR, resulting in determining that the inhibition of the phosphorylation of ERK pathway is a possible mechanism behind the observed anticancer activity of **6g**. Molecular modeling techniques have been utilized on the designed thiazolidines confirm the observed activity. A QSAR study shows that the electron deficient aryl rings attached to the thiazolidine core ring might enhance their corresponding activity, and that is confirmed by the reported activity. The molecular docking study has emphasized the importance of attaching an electron withdrawing group to benzylidene moiety and existence of the exocyclic imine group. Thus, the molecular modeling techniques provide a guide to validate and confirm the observed activity.

3.1. Material and methods

3.1.1. Chemistry

All reagents were purchased from commercial suppliers and were used as received unless otherwise indicated. Reactions were performed in oven-dried glassware (24 h at 120 °C). Analytical thin layer chromatography (TLC) was performed on silica gel 60F254 aluminum precoated plates (0.25 mm layer) and were visualized using UV light at 254 nm. All chromatographic purifications were performed using the flash chromatography method on silica gel (200–400 mesh). ^{1}H and ^{13}C NMR (δ in ppm) spectra were recorded in $CDCl_3$ (unless otherwise noted) at 500 and 125.8 MHz, respectively (unless otherwise noted). Residual $CHCl_3$ ($\delta = 7.26$) as reference for ^{1}H NMR and carbon absorption of $CDCl_3$ ($\delta = 77.0$) as internal reference for ^{13}C NMR were used. Data are reported as s = singlet, d = doublet, t = triplet, q = quartet, dd = doublet of doublets, dt = doublet of triplets, td = triplet of doublets, tt = triplet of triplets, m = multiplet. Infrared spectra were recorded neat using an ATR instrument. High resolution mass spectra (HR-MS) were acquired in the Shimadzu Center for Advanced Analytical Chemistry using electrospray ionization with mass being measured using TOF.

3.1.1.1. Synthesis of 4-(4-bromophenyl)-2-methylbut-3-yn-2-amine (9). To an oven-dried flask, 2-methylbut-3-yn-2-amine (**7**) (25 mmol, 1.0 equiv, 2.1 g), 1-bromo-4-iodobenzene (**8**) (27.5 mmol, 1.1 equiv, 7.9 g), $PdCl_2(PPh_3)_2$ (0.5 mmol, 2.0 mol%, 0.35 g), CuI (1.0 mmol, 4.0 mol%, 0.2 g) and then THF/TEA mixture (4:1, 60 ml:15 ml) were added. The reaction mixture was stirred at room temperature under argon for 24 h. Ammonium chloride (20 ml) was used to quench the reaction, followed by extraction using ether (3 × 15 ml), then the combined organic extracts were further washed with brine solution (15 ml) and dried over sodium sulfate. The solvent was removed by rotary evaporation and then the crude residue was subjected to silica gel chromatography using 50% ethyl acetate in hexanes to afford the desired 4-(4-bromophenyl)-2-methylbut-3-yn-2-amine (brown oil, 3.2 g, 55%).[76] ^{1}H NMR (500 MHz, $CDCl_3$) δ 7.43–7.29 (m, 2H), 7.27–7.12 (m, 2H), 1.84 (s, 2H), 1.42 (s, 3H), 1.41 (s, 3H). ^{13}C NMR (126 MHz, $CDCl_3$) δ 133.0, 131.5, 128.6, 128.5, 122.4, 122.0, 98.1, 79.2, 45.8, 31.7. FT-IR (neat, cm^{-1}): 3359, 3281, 2929, 2867, 2221, 1482, 1261, 1170, 818.

3.1.1.2. Synthesis of thiazolidines 6a-i. **General procedure:** To vigorously stirred silica gel (1.75 g) in 25 ml Erlenmeyer Flask, 4-(4-bromophenyl)-2-methylbut-3-yn-2-amine (**8**) (0.24 g, 1.0 mmol, 1.0 equiv) and the corresponding phenyl isothiocyanates (0.12–0.22 g, 1.0 mmol, 1.0 equiv) were added, then stirred the slurry at 65 °C for 24 h. The reaction was monitored by TLC (by taking a small portion of silica gel mixture and adding few drops of dichloromethane). The slurry was subjected to the flash column chromatography to afford the desired products which were further crystalized using appropriate solvents to isolate the crystalized products in high grade of purity for biological examinations.

(*Z*)-5-((*Z*)-4-bromobenzylidene)-*N*-(4-bromophenyl)-4,4-dimethylthiazolidin-2-imine (**6a**): Obtained by using *p*-bromophenyl isothiocyanate (0.22 g, 1.0 mmol, 1.0 equiv) as colorless needles (0.25 g, 55%, m.p. 226–229 °C) by ethanolic crystallization of white solid (0.35 g, 77%) isolated by flash chromatography using 15% ethyl acetate in hexanes. ^{1}H NMR (500 MHz, $CDCl_3$) δ 7.45–7.32 (m, 4H), 7.11–7.05 (m, 2H), 6.97 (d, $J = 8.1$ Hz, 2H), 6.32 (s, 1H), 1.45 (s, 6H). ^{13}C NMR (126 MHz, $CDCl_3$) δ 165.8, 157.9, 144.0, 135.2, 132.2, 131.7, 129.5, 123.5, 120.8, 117.6, 116.5, 80.1, 30.4. FT-IR (neat, cm^{-1}): 3060, 2965, 2846, 2770, 1644, 1613, 1577, 1435, 1166, 840. HRMS (*m/z*): calc for $C_{18}H_{17}N_2SBr_2$ $[M+1]^+$ 450.9474 found 450.9474.

(*Z*)-5-((*Z*)-4-bromobenzylidene)-*N*-(4-chlorophenyl)-4,4-dimethylthiazolidin-2-imine (6b): Obtained by using *p*-chlorophenyl isothiocyanate (0.17 g, 1.0 mmol, 1.0 equiv) as colorless needles (0.20 g, 50%, m.p. 196–198 °C) by toluene crystallization of white solid (0.30 g, 75%) isolated by flash chromatography using 15% ethyl acetate in hexanes. ^{1}H NMR (500 MHz, $CDCl_3$) δ 7.42–7.36 (m, 2H), 7.25–7.16 (m, 2H), 7.13–7.05 (m, 2H), 7.04–6.98 (m, 2H), 6.32 (s, 1H), 1.45 (s, 6H). ^{13}C NMR (126 MHz, $CDCl_3$) δ 176.6, 156.6, 145.6, 144.0, 135.2, 131.7, 129.5, 129.3, 129.1, 128.8, 128.3, 125.4, 123.1, 120.8, 117.5, 69.9, 30.4. FT-IR (neat, cm^{-1}): 3062, 3021, 2964, 2867, 2854, 1645, 1583, 1505,1166, 847. HRMS (*m/z*): calc for $C_{18}H_{17}N_2SClBr$ $[M+1]^+$ 406.9979 found 406.9954.

(Z)-5-((*Z*)-4-bromobenzylidene)-*N*-(4-fluorophenyl)-4,4-dimethylthiazolidin-2-imine (**6c**): Obtained by using *p*-fluorophenyl isothiocyanate (0.18 g, 1.2 mmol, 1.2 equiv) as colorless needles (0.18 g, 46%, m.p. 222–224 °C) by toluene crystallization of white solid (0.30 g, 77%) isolated by flash chromatography using 15% ethyl acetate in hexanes. ^{1}H NMR (500 MHz, $CDCl_3$) δ 7.44–7.34 (m, 2H), 7.15–7.01 (m, 4H), 7.00–6.91 (m, 2H), 6.32 (s, 1H), 1.46 (s, 6H). ^{13}C NMR (126 MHz, $CDCl_3$) δ 158.4, 145.9, 143.7, 135.3, 131.7, 129.4, 129.1, 128.3, 125.4, 123.3, 123.2, 120.7, 117.4, 115.9, 115.8, 71.5, 30.4. FT-IR (neat, cm^{-1}): 3061, 3019, 2990, 2948, 2868, 1649, 1615, 1248, 1175, 850. HRMS (*m/z*): calc for $C_{18}H_{17}N_2SFBr$ $[M+1]^+$ 391.0274 found 391.0264.

(*Z*)-5-((*Z*)-4-bromobenzylidene)-4,4-dimethyl-*N*-(4-nitrophenyl)thiazolidin-2-imine (6d): Obtained by using *p*-nitrophenyl isothiocyanate (0.22 g, 1.2 mmol, 1.2 equiv) as shiny yellow crystals (0.11 g, 30%, m.p. 212–214 °C) by methanolic crystallization of the yellow crude product (0.36 g, 95%). ^{1}H NMR (500 MHz, $CDCl_3$) δ 8.19–8.09 (m, 2H), 7.47–7.35 (m, 2H), 7.26 (d, $J = 8.5$ Hz, 2H), 7.10–7.02 (m, 2H), 6.38 (d, $J = 1.4$ Hz, 1H), 1.51 (s, 3H), 1.50 (s, 3H). ^{13}C NMR (126 MHz, $CDCl_3$) δ 169.9, 167.8, 150.9, 143.1, 135.3, 131.8, 129.4, 129.1, 128.3, 125.4, 120.9, 118.2, 67.5, 30.3. FT-IR (neat, cm^{-1}): 3079, 3037, 2961, 2870, 2819, 1648, 1615, 1486, 1379, 1248, 1106, 851. HRMS (*m/z*): calc for $C_{18}H_{17}N_3O_2SBr$ $[M+1]^+$ 418.0213 found 418.0219.

(*Z*)-5-((*Z*)-4-bromobenzylidene)-4,4-dimethyl-*N*-phenylthiazolidin-2-imine (6e): Obtained by using phenyl isothiocyanate (0.12 g, 1.0 mmol, 1.0 equiv) as tiny colorless needles (0.20 g, 54%, m.p. 216–220 °C) by toluene crystallization of the white solid (0.30 g, 80%) isolated by flash chromatography using 15% ethyl acetate in hexanes.

^{1}H NMR (500 MHz, $CDCl_3$) δ 7.43–7.36 (m, 2H), 7.30–7.24 (m, 2H), 7.17 (d, $J = 7.9$ Hz, 2H), 7.12–7.09 (m, 2H), 7.04 (tq, $J = 7.4$, 1.1 Hz, 1H), 6.33 (s, 1H), 1.49 (s, 6H). ^{13}C NMR (126 MHz, $CDCl_3$) δ 153.9, 153.0, 150.7, 135.5, 131.7, 129.4, 129.2, 123.7, 121.3, 120.5, 117.1, 106.3, 100.0, 48.7, 30.5. FT-IR (neat, cm^{-1}): 3017, 2963, 2855, 2800, 1652, 1615, 1587, 1483, 1195, 836. HRMS (*m/z*): calc for $C_{18}H_{18}N_2SBr$ $[M+1]^+$ 373.0354 found 373.0369.

(*Z*)-5-((*Z*)-4-bromobenzylidene)-4,4-dimethyl-*N*-(p-tolyl)thiazolidin-2-imine (6f): Obtained by using *p*-tolyl isothiocyanate (0.15 g, 1.0 mmol, 1.0 equiv) as colorless powders (0.13 g, 34%, m.p. 206–208 °C) by toluene crystallization of white solid (0.30 g, 78%) isolated by flash chromatography using 20% ethyl acetate in hexanes. ^{1}H NMR (500 MHz, $CDCl_3$) δ 7.40 (ddd, J = 8.8, 4.1, 1.8 Hz, 2H), 7.17–7.01 (m, 6H), 6.34 (s, 1H), 2.30 (s, 3H), 1.5 (s, 6H).^{13}C NMR (126 MHz, $CDCl_3$) δ 171.1, 142.1, 135.6, 133.5, 131.6, 129.8, 129.4, 127.3, 121.5, 120.5, 117.0, 110.8, 70.0, 30.5, 21.0. FT-IR (neat, cm^{-1}): 3089, 3022, 3010, 2905, 1641, 1601, 1506, 1484, 1247, 1173, 831. HRMS (*m/z*): calc for $C_{19}H_{20}N_2SBr$ $[M+1]^+$ 387.0499 found 387.0525.

(*Z*)-5-((*Z*)-4-bromobenzylidene)-*N*-(4-methoxy-2-nitrophenyl)-4,4-dimethylthiazolidin-2-imine (6g): Obtained by using 4-methoxy-2-nitrophenyl isothiocyanate (0.21 g, 1.0 mmol, 1.0 equiv) as yellow powder (0.20 g, 44%, m.p. 252–254 °C) by toluene crystallization of the yellow solid (0.42 g, 94%) isolated by flash chromatography using 15% ethyl acetate in hexanes. ^{1}H NMR (500 MHz, CDCl3) δ 8.63 (s, 1H), 7.60 (t, J = 2.9 Hz, 1H), 7.50–7.37 (m, 2H), 7.19 (dq, J = 9.4, 3.0 Hz, 1H), 7.18–7.06 (m, 1H), 6.39 (d, J = 2.4 Hz, 1H), 3.80 (d, J = 2.5 Hz, 2H), 1.53 (s, 3H), 1.52 (s, 3H). ^{13}C NMR (126 MHz, $CDCl_3$) δ 153.8, 146.8, 143.8, 135.7, 131.7, 129.3, 128.4, 124.3, 123.2, 120.6, 117.1, 108.1, 55.9, 30.4. FT-IR (neat, cm^{-1}): 3086, 3030, 3006, 2961, 2868, 2835, 1614, 1561, 1518, 1478, 1397, 1288, 1256, 882. HRMS (*m/z*): calc for $C_{18}H_{20}N_2BrS$ $[M+1]^+$ 373.0369 found 373.0354.

(*Z*)-5-((*Z*)-4-bromobenzylidene)-*N*-(3-chloro-4-methylphenyl)-4,4-dimethylthiazolidin-2-imine (6h): Obtained by using 3-chloro-4-methylphenyl isothiocyanate (0.18 g, 1.0 mmol, 1.0 equiv) as colorless powder (0.16 g, 40%, m.p. 208–210 °C) by toluene crystallization of white solid (0.33 g, 80%) isolated by flash chromatography using 15% ethyl acetate in hexanes. ^{1}H NMR (500 MHz, $CDCl_3$) δ 7.73 (s, 1H), 7.44–7.36 (m, 2H), 7.14–7.03 (m, 5H), 6.89 (dd, J = 8.2, 2.3 Hz, 1H), 6.33 (s, 1H), 2.29 (s, 3H), 1.48 (s, 6H). ^{13}C NMR (126 MHz, $CDCl_3$) δ 156.8, 144.6, 143.5, 135.1, 134.6, 131.7, 131.6, 131.4, 129.5, 128.3, 125.4, 122.6, 120.9, 120.4, 117.8, 70.0, 30.4, 19.6. FT-IR (neat, cm^{-1}): 3110, 3043, 3031, 2926, 2874, 1649, 1599, 1552, 1484, 1276, 1008, 850. HRMS (*m/z*): calc for $C_{19}H_{19}N_2SClBr$ $[M+1]^+$ 421.0135 found 421.0128.

(*Z*)-5-((*Z*)-4-bromobenzylidene)-*N*-(4-methoxyphenyl)-4,4-dimethylthiazolidin-2-imine (6i): Obtained by using 4-methoxyphenyl isothiocyanate (0.19 g, 1.0 mmol, 1.0 equiv) as shiny colorless needles (0.17 g, 42%, m.p. 170–172 °C) by toluene crystallization of the white solid (0.32 g, 85%) isolated by flash chromatography using 15% ethyl acetate in hexanes. ^{1}H NMR (500 MHz, $CDCl_3$) δ 7.41–7.34 (m, 2H), 7.15–7.02 (m, 4H), 6.84–6.76 (m, 2H), 6.31 (s, 1H), 3.75 (s, 3H), 1.46 (s, 6H). ^{13}C NMR (126 MHz, $CDCl_3$) δ 156.7, 156.6, 145.1, 138.3, 137.9, 135.4, 131.7, 129.4, 129.1, 128.3, 125.4, 123.9, 120.6, 117.2, 114.4, 71.8, 55.5, 30.5. FT-IR (neat, cm^{-1}): 3021, 2960, 2829, 2777, 2657, 1657, 1613, 1501, 1209, 850. HRMS (*m/z*): calc for $C_{19}H_{20}N_2OSBr$ $[M+1]^+$ 403.0474 found 403.0468.

3.1.2. X-ray study

The single crystal X-ray diffraction studies were carried out on a Bruker Kappa APEX-II CCD diffractometer at 293(2) K using monochromated Mo- Kα radiation (λ = 0.71073 Å) and a detector-to-crystal distance of 5.220 cm. A 0.35 × 0.10 × 0.047 mm colorless needle was mounted on a Cryoloop with Nujol oil. Data were collected in a hemisphere or full sphere of reciprocal space with 0.3° scans in ω for an exposure time of 30 s per frame up to a maximum 2θ value of 56.26°. A total of 3407 reflections were collected covering the indices, $-21 \leq h \leq 21$, $-7 \leq k \leq 7$, $-25 \leq l \leq 24$. 2759 reflections were found to be symmetry independent, with a Rint of 0.0234. Indexing and unit cell refinement indicated a monoclinic lattice. The space group was found to be P21/n. The measured intensities were corrected for Lorenz and polarization effects and were further corrected for absorption using the multi-scan method SCALE3 ABSPACK. Based on the data, a structural model was obtained by direct method using the Superflip subroutine implemented in the JANA2006 software package. The refinement was performed via full-matrix least-squares on F2 by using the JANA2006 software package. Crystallographic data are summarized in supporting information.

3.1.3. Molecular modeling studies

The methodology of 3D-pharmacophore modeling and 2D-DSAR studies is mentioned in the supplementary file.

3.1.4. Anti-tumor activity evaluation

3.1.4.1. Cell culture. ESCC cell lines (KYSE-30 and KYSE-150) were maintained as previously reported [89]. Two non-tumorigenic esophageal epithelial HET-1A and NES-G4T cell lines were cultured following the established procedure [90]. All cells were cultured at 37 °C in humidified air with 5% CO_2.

3.1.4.2. MTT assay. Cells were seeded into 96-well plates with 100 μL cell culture medium per well and incubated with different concentrations of thiazolidine compounds for 72 h 10 μL of 5 mg/ml 3-(4, 5-dimethylthiazol-2-yl)-2,5-diphenyl-tetrazolium bromide (MTT) was added into the cell culture medium and allowed to incubate at 37 °C in the dark for 3 h. Then, the cell culture medium was removed, and the formazan was dissolved in DMSO (150 μL/well). Absorbance measurement was conducted at 570 nm by SpectraMax i3 (Molecular Devices, CA). Relative cell viability and IC_{50} were calculated using GraphPad Prism 9 (GraphPad, USA).

3.1.4.3. Western blot. Cultured cells were treated with 10 μL of compound **9g** and incubated for 4 h, 8 h, and 12 h. Lysis of cells was performed using RIPA buffer supplemented with proteinase inhibitor cocktail. Pierce BCA protein assay kit (Thermo, US) was utilized for the determination of protein concentration. Primary antibodies used in this study were anti-AKT (1:1000, Cell Signaling Technology, US), anti-P-AKT (1:1000, Cell Signaling Technology, US), anti-p44/42 MAPK (1:1000, Cell Signaling Technology, US), and anti-P-p44/42 MAPK (1:1000, Cell Signaling Technology, US). Secondary antibodies included anti-rabbit IgG (1:5000, Cell Signaling Technology, US) and anti-mouse IgG (1:5000, Cell Signaling Technology, US). Images were obtained using ChemiDoc Imaging System (Bio-Rad, USA).

3.1.4.4. Cell death analysis. KYSE-30 and KYSE-150 cells were cultured in a growth medium for 24 h, followed by 10 μM **9g** treatment for 24 h, 48 h, and 72 h. For fixation, cells were incubated in 4% paraformaldehyde at room temperature for 20 min. Nuclei staining was attained by incubating cells in 1 μg/ml DAPI (Life Technologies Corporation, OR) in PBS containing 0.5% Triton X-100 in the dark for 10 min. After incubation, cells were washed with PBS. Nikon A1R HD25 laser scanning confocal, microscope with 60x objective (NA 1.4) (Nikon, Japan), was used to take nuclei images.

3.1.4.5. Statistical analysis. GraphPad Prism 9 (GraphPad, US) was used to perform statistical analyses. Data were recorded as the mean ± standard error of the mean (S.E.M). Differences were considered significant at a P value ≤ 0.05 in all cases.

Declaration of competing interest

The authors declare the following financial interests/personal relationships which may be considered as potential competing interests: Carl J. Lovely reports financial support was provided by National Science Foundation.

Data availability

Data will be made available on request.

Acknowledgements

This work has been supported by the Robert A. Welch Foundation (Y-1362, CJL), the NSF (CHE-1956328, CJL), the NIH (S10OD025230, PZ) and by instrumentation grants from the NSF (CHE-0234811 and CHE-0840509) for the purchase of the NMR spectrometers used in this research.

Appendix A. Supplementary data

Supplementary data to this article can be found online at https://doi.org/10.1016/j.ejmech.2022.114909.

References

[1] H. Sung, J. Ferlay, R.L. Siegel, M. Laversanne, I. Soerjomataram, A. Jemal, F. Bray, Global cancer statistics 2020: GLOBOCAN estimates of incidence and mortality worldwide for 36 cancers in 185 countries, CA. Cancer J. Clin. 71 (3) (2021) 209–249, https://doi.org/10.3322/caac.21660.
[2] R. Naresh, Y. Nazeer, S. Palani, In silico evaluation of modes of action of anticancer compounds on molecular targets for cancer, Med. Chem. Res. 22 (4) (2013) 1938–1947, https://doi.org/10.1007/s00044-012-0198-4.
[3] K. De Bock, M. Mazzone, P. Carmeliet, Antiangiogenic therapy, hypoxia, and metastasis: risky liaisons, or not? Nat. Rev. Clin. Oncol. 8 (2011) 393–404, https://doi.org/10.1038/nrclinonc.2011.83.
[4] S. Yang, J.J. Zhang, X.Y. Huang, Orai1 and STIM1 are critical for breast tumor cell migration and metastasis, Cancer Cell 15 (2) (2009) 124–134, https://doi.org/10.1016/j.ccr.2008.12.019.
[5] P.S. Steeg, Targeting metastasis, Nat. Rev. Cancer 16 (4) (2016) 201–218, https://doi.org/10.1038/nrc.2016.25.
[6] C.-N. Qian, Y. Mei, J. Zhang, Cancer metastasis: issues and challenges, Chin. J. Cancer 36 (1) (2017) 38, https://doi.org/10.1186/s40880-017-0206-7.
[7] 6-Oesophagus-fact-sheet.pdf (iarc.Fr).
[8] Z. Chen, X. Hu, Y. Wu, L. Cong, X. He, J. Lu, J. Feng, D. Liu, Long non-coding RNA XIST promotes the development of esophageal cancer by sponging MiR-494 to regulate CDK6 expression, Biomed. Pharmacother. 109 (2019) 2228–2236, https://doi.org/10.1016/j.biopha.2018.11.049.
[9] J. Li, T. Wang, L. Pei, J. Jing, W. Hu, T. Sun, H. Liu, Expression of VRK1 and the downstream gene BANF1 in esophageal cancer, Biomed. Pharmacother. (2017), https://doi.org/10.1016/j.biopha.2017.02.095.
[10] M. Arnold, J. Ferlay, M.I. Van Berge Henegouwen, I. Soerjomataram, Global burden of oesophageal and gastric cancer by histology and subsite in 2018, Gut 69 (9) (2020) 1564–1571, https://doi.org/10.1136/gutjnl-2020-321600.
[11] M.J.D. Arnal, Á.F. Arenas, Á.L. Arbeloa, Esophageal cancer: risk factors, screening and endoscopic treatment in western and eastern countries, World J. Gastroenterol. 21 (26) (2015) 7933–7943, https://doi.org/10.3748/wjg.v21.i26.7933.
[12] M. di Pietro, M.I. Canto, R.C. Fitzgerald, Endoscopic management of early adenocarcinoma and squamous cell carcinoma of the esophagus: screening, diagnosis, and therapy, Gastroenterology 154 (2) (2018) 421–436, https://doi.org/10.1053/j.gastro.2017.07.041.
[13] J. Ying, M. Zhang, X. Qiu, Y. Lu, The potential of herb medicines in the treatment of esophageal cancer, Biomed. Pharmacother. 103 (2018) 381–390, https://doi.org/10.1016/j.biopha.2018.04.088.
[14] K. Higuchi, W. Koizumi, S. Tanabe, T. Sasaki, C. Katada, M. Azuma, K. Nakatani, K. Ishido, A. Naruke, T. Ryu, Current management of esophageal squamous-cell carcinoma in Japan and other countries, Gastrointest. Cancer Res. 3 (4) (2009) 153–161.
[15] Y.-S. Chang, J.-C. Liu, H.-Q. Fu, B.-T. Yu, S.-B. Zou, Q.-C. Wu, L. Wan, Roles of targeting ras/raf/MEK/ERK signaling pathways in the treatment of esophageal carcinoma, Yao Xue Xue Bao 48 (5) (2013) 635–641.
[16] S.-T. Zheng, Q. Huo, A. Tuerxun, W.-J. Ma, G.-D. Lv, C.-G. Huang, Q. Liu, X. Wang, R.-Y. Lin, I. Sheyhidin, X.-M. Lu, The expression and activation of ERK/MAPK pathway in human esophageal cancer cell line EC9706, Mol. Biol. Rep. 38 (2) (2011) 865–872, https://doi.org/10.1007/s11033-010-0178-z.
[17] M. Yanchun, W. Yi, W. Lu, Q. Yu, Y. Jian, K. Pengzhou, Y. Ting, L. Hongyi, W. Fang, C. Xiaolong, C. Yongping, Triptolide prevents proliferation and migration of esophageal squamous cell cancer via MAPK/ERK signaling pathway, Eur. J. Pharmacol. 851 (2019) 43–51, https://doi.org/10.1016/j.ejphar.2019.02.030.
[18] H. Shi, Q. Ju, Y. Mao, Y. Wang, J. Ding, X. Liu, X. Tang, C. Sun, TAK1 phosphorylates RASSF9 and inhibits esophageal squamous tumor cell proliferation by targeting the RAS/MEK/ERK Axis, Adv. Sci. 8 (5) (2021), 2001575, https://doi.org/10.1002/advs.202001575.
[19] H. Wang, Y. Zhang, H. Yun, S. Chen, Y. Chen, Z. Liu, ERK expression and its correlation with STAT1 in esophageal squamous cell carcinoma, Oncotarget 8 (28) (2017) 45249–45258, https://doi.org/10.18632/oncotarget.16902.
[20] M. Soares-Silva, F.F. Diniz, G.N. Gomes, D. Bahia, The mitogen-activated protein kinase (MAPK) pathway: role in immune evasion by trypanosomatids, Front. Microbiol. 7 (2016) 183, https://doi.org/10.3389/fmicb.2016.00183.
[21] G.L. Johnson, R. Lapadat, Mitogen-activated protein kinase pathways mediated by ERK, JNK, and P38 protein kinases, Science 298 (5600) (2002) 1911–1912, https://doi.org/10.1126/science.1072682.
[22] D.M. Owens, S.M. Keyse, Differential regulation of MAP kinase signalling by dual-specificity protein phosphatases, Oncogene 26 (22) (2007) 3203–3213, https://doi.org/10.1038/sj.onc.1210412.
[23] Y. Zhang, C. Dong, Regulatory mechanisms of mitogen-activated kinase signaling, Cell. Mol. Life Sci. 64 (21) (2007) 2771–2789, https://doi.org/10.1007/s00018-007-7012-3.
[24] R. Mandal, M. Raab, Y. Matthess, S. Becker, R. Knecht, K. Strebhardt, PERK 1/2 inhibit caspase-8 induced apoptosis in cancer cells by phosphorylating it in a cell cycle specific manner, Mol. Oncol. 8 (2) (2014) 232–249, https://doi.org/10.1016/j.molonc.2013.11.003.
[25] C. Dong, R.J. Davis, R.A. Flavell, MAP kinases in the immune response, Annu. Rev. Immunol. 20 (1) (2002) 55–72, https://doi.org/10.1146/annurev.immunol.20.091301.131133.
[26] R.J. Roskoski, ERK1/2 MAP kinases: structure, function, and regulation, Pharmacol. Res. 66 (2) (2012) 105–143, https://doi.org/10.1016/j.phrs.2012.04.005.
[27] I. Wortzel, R. Seger, The ERK cascade: distinct functions within various subcellular organelles, Genes Cancer 2 (3) (2011) 195–209, https://doi.org/10.1177/1947601911407328.
[28] H.M. Chin, D.K. Lai, G.S. Falchook, Extracellular signal-regulated kinase (ERK) inhibitors in oncology clinical trials, J. Immunother. Precis. Oncol. 2 (1) (2020) 10–16, https://doi.org/10.4103/JIPO.JIPO_17_18.
[29] A. Portelinha, S. Thompson, R.A. Smith, M. Da Silva Ferreira, Z. Asgari, A. Knezevic, V. Seshan, E. de Stanchina, S. Gupta, L. Denis, A. Younes, S. Reddy, ASN007 is a selective ERK1/2 inhibitor with preferential activity against RAS-and RAF-mutant tumors, Cell Reports Med 2 (7) (2021), 100350, https://doi.org/10.1016/j.xcrm.2021.100350.
[30] L. Galluzzi, M.C. Maiuri, I. Vitale, H. Zischka, M. Castedo, L. Zitvogel, G. Kroemer, Cell death modalities: classification and pathophysiological implications, Cell DeathDiffer 14 (2007) 1237–1243, https://doi.org/10.1038/sj.cdd.4402148.
[31] G. Kroemer, L. Galluzzi, P. Vandenabeele, J. Abrams, E.S. Alnemri, E.H. Baehrecke, M.V. Blagosklonny, W.S. El-Deiry, P. Golstein, D.R. Green, M. Hengartner, R. A. Knight, S. Kumar, S.A. Lipton, W. Malorni, G. Nuñez, M.E. Peter, J. Tschopp, J. Yuan, M. Piacentini, B. Zhivotovsky, G. Melino, Classification of cell death: recommendations of the nomenclature committee on cell death 2009, Cell Death Differ. 16 (2009) 3–11, https://doi.org/10.1038/cdd.2008.150.
[32] L. Galluzzi, J.M. Bravo-San Pedro, I. Vitale, S.A. Aaronson, J.M. Abrams, D. Adam, E.S. Alnemri, L. Altucci, D. Andrews, M. Annicchiarico-Petruzzelli, E.H. Baehrecke, N.G. Bazan, M.J. Bertrand, K. Bianchi, M.V. Blagosklonny, K. Blomgren, C. Borner, D.E. Bredesen, C. Brenner, M. Campanella, E. Candi, F. Cecconi, F.K. Chan, N. S. Chandel, E.H. Cheng, J.E. Chipuk, J.A. Cidlowski, A. Ciechanover, T.M. Dawson, V.L. Dawson, V. De Laurenzi, R. De Maria, K.M. Debatin, N. Di Daniele, V.M. Dixit, B.D. Dynlacht, W.S. El-Deiry, G.M. Fimia, R.A. Flavell, S. Fulda, C. Garrido, M. L. Gougeon, D.R. Green, H. Gronemeyer, G. Hajnoczky, J.M. Hardwick, M. O. Hengartner, H. Ichijo, B. Joseph, P.J. Jost, T. Kaufmann, O. Kepp, D.J. Klionsky, R.A. Knight, S. Kumar, J.J. Lemasters, B. Levine, A. Linkermann, S.A. Lipton, R. A. Lockshin, C. López-Otín, E. Lugli, F. Madeo, W. Malorni, J.C. Marine, S. J. Martin, J.C. Martinou, J.P. Medema, P. Meier, S. Melino, N. Mizushima, U. Moll, C. Muñoz-Pinedo, G. Nuñez, A. Oberst, T. Panaretakis, J.M. Penninger, M.E. Peter, M. Piacentini, P. Pinton, J.H. Prehn, H. Puthalakath, G.A. Rabinovich, K. S. Ravichandran, R. Rizzuto, C.M. Rodrigues, D.C. Rubinsztein, T. Rudel, Y. Shi, H. U. Simon, B.R. Stockwell, G. Szabadkai, S.W. Tait, H.L. Tang, N. Tavernarakis, Y. Tsujimoto, T. Vanden Berghe, P. Vandenabeele, A. Villunger, E.F. Wagner, H. Walczak, E. White, W.G. Wood, J. Yuan, Z. Zakeri, B. Zhivotovsky, G. Melino, G. Kroemer, Essential versus accessory aspects of cell death: recommendations of the NCCD 2015, Cell Death Differ. 22 (2015) 58–73, https://doi.org/10.1038/cdd.2014.137.
[33] B. Méry, J.B. Guy, A. Vallard, S. Espenel, D. Ardail, C. Rodriguez-Lafrasse, C. Rancoule, N. Magné, In vitro cell death determination for drug discovery: a landscape review of real issues, J. Cell Death 10 (2017) 1–8, https://doi.org/10.1177/1179670717691251.
[34] M. Ocker, M. Höpfner, Apoptosis-modulating drugs for improved cancer therapy, Eur. Surg. Res. 48 (3) (2012) 111–120, https://doi.org/10.1159/000336875.
[35] H. Wajant, K. Pfizenmaier, P. Scheurich, Tumor necrosis factor signaling, Cell Death Differ. 10 (1) (2003) 45–65, https://doi.org/10.1038/sj.cdd.4401189.
[36] V. Baud, M. Karin, Signal transduction by tumor necrosis factor and its relatives, Trends Cell Biol. 11 (9) (2001) 372–377, https://doi.org/10.1016/s0962-8924(01)02064-5.
[37] C.M. Pfeffer, A.T.K. Singh, Apoptosis: a target for anticancer therapy, Int. J. Mol. Sci. 19 (2) (2018) 448, https://doi.org/10.3390/ijms19020448.
[38] S.D. Kobayashi, J.M. Voyich, A.R. Whitney, F.R. DeLeo, Spontaneous neutrophil apoptosis and regulation of cell survival by granulocyte macrophage-colony stimulating factor, J. Leukoc. Biol. 78 (6) (2005) 1408–1418, https://doi.org/10.1189/jlb.0605289.
[39] M.L. Wang, R. Tuli, P.A. Manner, P.F. Sharkey, D.J. Hall, R.S. Tuan, Direct and indirect induction of apoptosis in human mesenchymal stem cells in response to titanium particles, J. Orthop. Res. 21 (4) (2003) 697–707, https://doi.org/10.1016/S0736-0266(02)00241-3.
[40] D. Hanahan, R.A. Weinberg, The hallmarks of cancer, Cell 100 (1) (2000) 57–70, https://doi.org/10.1016/S0092-8674(00)81683-9.

[41] D. Hanahan, R.A. Weinberg, Hallmarks of cancer: the next generation, Cell 144 (5) (2011) 646–674, https://doi.org/10.1016/j.cell.2011.02.013.
[42] C.J. Norbury, I.D. Hickson, Cellular responses to DNA damage, Annu. Rev. Pharmacol. Toxicol. 41 (2001) 367–401, https://doi.org/10.1146/annurev.pharmtox.41.1.367.
[43] M.A. Gouda, A.A. Abu-Hashem, Synthesis, characterization, antioxidant and antitumor evaluation of some new thiazolidine and thiazolidinone derivatives, Arch. Pharm. (Weinheim) 344 (2011) 170–177, https://doi.org/10.1002/ardp.201000165.
[44] S. Nishida, H. Maruoka, Y. Yoshimura, T. Goto, R. Tomita, E. Masumoto, F. Okabe, K. Yamagata, T. Fujioka, Synthesis and biological activities of some new thiazolidine derivatives containing pyrazole ring system, J. Heterocycl. Chem. 49 (2) (2012) 303–309, https://doi.org/10.1002/jhet.834.
[45] Q. Zhang, H. Zhou, S. Zhai, B. Yan, Natural product-inspired synthesis of thiazolidine and thiazolidinone compounds and their anticancer activities, Curr. Pharmaceut. Des. 16 (16) (2010) 1826–1842, https://doi.org/10.2174/138161210791208983.
[46] D. Havrylyuk, B. Zimenkovsky, O. Vasylenko, R. Lesyk, Synthesis and anticancer and antiviral activities of new 2-pyrazoline-substituted 4-thiazolidinones, J. Heterocycl. Chem. 50 (S1) (2013) E55–E62, https://doi.org/10.1002/jhet.1056.
[47] D. Osmaniye, S. Levent, C.M. Ardıç, Ö. Atlı, Y. Özkay, Z.A. Kaplancıklı, Synthesis and anticancer activity of some novel benzothiazole-thiazolidine derivatives, Phosphorus, Sulfur Silicon Relat. Elem. 193 (4) (2018) 249–256, https://doi.org/10.1080/10426507.2017.1395878.
[48] M.S.A. El-Gaby, Z.H. Ismail, S.M. Abdel-Gawad, H.M. Aly, M.M. Ghorab, Synthesis of thiazolidine and thiophene derivatives for evaluation as anticancer agents, Phosphorus, Sulfur Silicon Relat. Elem. 184 (10) (2009) 2645–2654, https://doi.org/10.1080/10426500802561096.
[49] M.N. Aziz, A. Patel, A. Iskander, A. Chini, D. Gout, S.S. Mandal, C.J. Lovely, One-pot synthesis of novel 2-imino-5-arylidine-thiazolidine analogues and evaluation of their anti-proliferative activity against MCF7 breast cancer cell line, Molecules 27 (3) (2022) 841, https://doi.org/10.3390/molecules27030841.
[50] R.P. Singh, M.N. Aziz, D. Gout, W. Fayad, M.A. El-Manawaty, C.J. Lovely, Novel thiazolidines: synthesis, antiproliferative properties and 2D-QSAR studies, Bioorg. Med. Chem. 27 (20) (2019), https://doi.org/10.1016/j.bmc.2019.115047.
[51] R. Morigi, A. Locatelli, A. Leoni, M. Rambaldi, Recent patents on thiazole derivatives endowed with antitumor activity, Recent Pat. Anti-Cancer Drug Discov. 10 (2015), https://doi.org/10.2174/1574892810666150708110432.
[52] Y. Yang, M. Cui, Radiolabeled bioactive benzoheterocycles for imaging β-amyloid plaques in alzheimer's disease, Eur. J. Med. Chem. 87 (2014) 703–721, https://doi.org/10.1016/j.ejmech.2014.10.012.
[53] K. Beulah, D.A.R. Kumar, B. Lingaiah, P. Rao, B. Narsaiah, A. Reddy, U. Murty, Design, synthesis and biological evaluation of benzimidazole-pyridine- piperidine hybrids as a new class of potent antimicrobial agents, Lett. Drug Des. Discov. 12 (2015) 38–45, https://doi.org/10.2174/1570180811666140725185713.
[54] L. Wang, C. Guo, X. Li, X. Yu, X. Li, K. Xu, B. Jiang, X. Jia, C. Li, D. Shi, Design, synthesis and biological evaluation of bromophenol-thiazolylhydrazone hybrids inhibiting the interaction of translation initiation factors EIF4E/EIF4G as multifunctional agents for cancer treatment, Eur. J. Med. Chem. 177 (2019) 153–170, https://doi.org/10.1016/j.ejmech.2019.05.044.
[55] M.D. Altıntop, B. Sever, G. Akalın Çiftçi, A. Özdemir, Design, synthesis, and evaluation of a new series of thiazole-based anticancer agents as potent Akt inhibitors, Molecules 23 (6) (2018), https://doi.org/10.3390/molecules23061318.
[56] D. Havrylyuk, O. Roman, R. Lesyk, Synthetic approaches, structure activity relationship and biological applications for pharmacologically attractive pyrazole/pyrazoline–thiazolidine-based hybrids, Eur. J. Med. Chem. 113 (2016) 145–166, https://doi.org/10.1016/j.ejmech.2016.02.030.
[57] T.A. Farghaly, E.M.H. Abbas, A.M. Al-Soliemy, R. Sabour, M.R. Shaaban, Novel sulfonyl thiazolyl-hydrazone derivatives as EGFR inhibitors: design, synthesis, biological evaluation and molecular docking studies, Bioorg. Chem. 121 (2022), 105684, https://doi.org/10.1016/j.bioorg.2022.105684.
[58] P.C. Sharma, K.K. Bansal, A. Sharma, D. Sharma, A. Deep, Thiazole-containing compounds as therapeutic targets for cancer therapy, Eur. J. Med. Chem. 188 (2020), 112016, https://doi.org/10.1016/j.ejmech.2019.112016.
[59] E. Zeytün, D.M. Altıntop, B. Sever, A. Özdemir, E.D. Ellakwa, Z. Ocak, I.H. Ciftci, M. Otsuka, M. Fujita, O.M. Radwan, A new series of antileukemic agents: design, synthesis, *in vitro* and *in silico* evaluation of thiazole-based ABL1 kinase inhibitors, Anti Cancer Agents Med. Chem. 21 (9) (2021) 1099–1109, https://doi.org/10.2174/1871520620666200824100408.
[60] A.A. Geronikaki, A.A. Lagunin, D.I. Hadjipavlou-Litina, P.T. Eleftheriou, D. A. Filimonov, V.V. Poroikov, I. Alam, A.K. Saxena, Computer-aided discovery of anti-inflammatory thiazolidinones with dual cyclooxygenase/lipoxygenase inhibition, J. Med. Chem. 51 (6) (2008) 1601–1609, https://doi.org/10.1021/jm701496h.
[61] L. Ma, C. Xie, Y. Ma, J. Liu, M. Xiang, X. Ye, H. Zheng, Z. Chen, Q. Xu, T. Chen, J. Chen, J. Yang, N. Qiu, G. Wang, X. Liang, A. Peng, S. Yang, Y. Wei, L. Chen, Synthesis and biological evaluation of novel 5-benzylidenethiazolidine-2,4- dione derivatives for the treatment of inflammatory diseases, J. Med. Chem. 54 (7) (2011) 2060–2068, https://doi.org/10.1021/jm1011534.
[62] C.D. Barros, A.A. Amato, T.B. de Oliveira, K.B.R. Iannini, A. L. da Silva, T. G. da Silva, E.S. Leite, M.Z. Hernandes, M. Alves de Lima, C. do, S.L. Galdino, F. de A. R. Neves, I. da R. Pitta, Synthesis and anti-inflammatory activity of new arylidene-thiazolidine-2,4-diones as PPARgamma ligands, Bioorg. Med. Chem. 18 (11) (2010) 3805–3811, https://doi.org/10.1016/j.bmc.2010.04.045.
[63] P.A. Datar, S.B. Aher, Design and synthesis of novel thiazolidine-2,4-diones as hypoglycemic agents, J. Saudi Chem. Soc. 20 (2016) S196–S201, https://doi.org/10.1016/j.jscs.2012.10.010.
[64] I.R. Siddiqui, P.K. Singh, J. Singh, J. Singh, Synthesis and fungicidal activity of novel 4,4′-bis(2″ -Aryl-5″-Methyl/Unsubstituted-4″-Oxo-Thiazolidin-3″-Yl) bibenzyl, J. Agric. Food Chem. 51 (24) (2003) 7062–7065, https://doi.org/10.1021/jf0342324.
[65] M.R. Shiradkar, M. Ghodake, K.G. Bothara, S.V. Bhandari, A. Nikalje, K.C. Akula, N.C. Desai, P.J. Burange, Synthesis and anticonvulsant activity of clubbed thiazolidinone-barbituric acid and thiazolidinone-triazole derivatives, ARKIVOC (Gainesville, FL, U. S.) 2007 (2007), https://doi.org/10.3998/ark.5550190.0008.e08.
[66] D.R.M. Moreira, S.P.M. Costa, M.Z. Hernandes, M.M. Rabello, G.B. de Oliveira Filho, C.M.L. de Melo, L.F. da Rocha, C.A. de Simone, R.S. Ferreira, J.R.B. Fradico, C.S. Meira, E.T. Guimarães, R.M. Srivastava, V.R.A. Pereira, M.B.P. Soares, A.C. L. Leite, Structural investigation of anti-trypanosoma cruzi 2-iminothiazolidin-4-ones allows the identification of agents with efficacy in infected mice, J. Med. Chem. 55 (24) (2012) 10918–10936, https://doi.org/10.1021/jm301518v.
[67] F.K. Zehetmeyr, M.A.M.P. da Silva, K.M. Pereira, M.E.A. Berne, W. Cunico, J.C. J. Campos, D.P. Gouvea, P. da Silva Nascente, S. de Oliveira Hübner, G.M. Siqueira, Ovicidal in vitro activity of 2-aryl-3-(2-Morpholinoethyl)Thiazolidin-4-ones and 2-aryl-3-(3-Morpholinopropyl)Thiazolidin-4-ones against fasciola hepatica (linnaeus, 1758), Exp. Parasitol. 192 (2018) 60–64, https://doi.org/10.1016/j.exppara.2018.07.012.
[68] S. Jiang, S.R. Tala, H. Lu, N.E. Abo-Dya, I. Avan, K. Gyanda, L. Lu, A.R. Katritzky, A.K. Debnath, Design, synthesis, and biological activity of novel 5-((arylfuran/1H-Pyrrol-2-Yl)Methylene)-2-Thioxo-3-(3-(Trifluoromethyl)Phenyl)Thiazolidin-4-Ones as HIV-1 fusion inhibitors targeting Gp41, J. Med. Chem. 54 (2) (2011) 572–579, https://doi.org/10.1021/jm101014v.
[69] M.L. Barreca, J. Balzarini, A. Chimirri, E. De Clercq, L. De Luca, H.D. Höltje, M. Höltje, A.M. Monforte, P. Monforte, C. Pannecouque, A. Rao, M. Zappalà, Design, synthesis, structure-activity relationships, and molecular modeling studies of 2,3-diaryl-1,3-thiazolidin-4-ones as potent anti-HIV agents, J. Med. Chem. 45 (24) (2002) 5410–5413, https://doi.org/10.1021/jm020977+.
[70] T. Rajeswari, T. Rekha, G. Dinneswara Reddy, A. Padmaja, V. Padmavathi, Synthesis and antibacterial activity of benzazolyl azolyl sulfamoyl acetamides, J. Heterocycl. Chem. 56 (9) (2019) 2449–2459, https://doi.org/10.1002/jhet.3634.
[71] A. Deep, P. Kumar, B. Narasimhan, K. Ramasamy, V. Mani, R.K. Mishra, A.B. A. Majeed, Synthesis, antimicrobial, anticancer evaluation of 2-(aryl)-4-thiazolidinone derivatives and their QSAR studies, Curr. Top. Med. Chem. 15 (11) (2015) 990–1002, https://doi.org/10.2174/1568026615666150317221849.
[72] R.P. Singh, D. Gout, C.J. Lovely, Tandem thioacylation-intramolecular hydrosulfenylation of propargyl amines – rapid access to 2-aminothiazolidines, Eur. J. Org. Chem. 8 (2019) 1726–1740, https://doi.org/10.1002/ejoc.201801505.
[73] R.P. Singh, M.N. Aziz, D. Gout, W. Fayad, M.A. El-Manawaty, C.J. Lovely, Novel thiazolidines: synthesis, antiproliferative properties and 2D-QSAR studies, Bioorg. Med. Chem. 27 (20) (2019), 115047, https://doi.org/10.1016/j.bmc.2019.115047.
[74] M.N. Aziz, A. Patel, A. Iskander, A. Chini, D. Gout, S.S. Mandal, C.J. Lovely, One-pot synthesis of novel 2-imino-5-arylidine-thiazolidine analogues and evaluation of their anti-proliferative activity against MCF7 breast cancer cell line, Molecules 27 (3) (2022) 841, https://doi.org/10.3390/molecules27030841.
[75] A.M. Srour, S.S. Panda, A.M. M Salman, M.A. El-Manawaty, R.F. George, E. M. Shalaby, A.N. Fitch, N.G. Fawzy, A.S. Girgis, Synthesis & molecular modeling studies of bronchodilatory active indole-pyridine conjugates, Future Med. Chem. 10 (15) (2018) 1787–1804, https://doi.org/10.4155/fmc-2018-0039.
[76] J. Ying, Z. Le, X.-F. Wu, Benzene-1,3,5-Triyl triformate (TFBen)-Promoted palladium-catalyzed carbonylative synthesis of 2-oxo-2,5-dihydropyrroles from propargyl amines, Org. Lett. 22 (1) (2020) 194–198, https://doi.org/10.1021/acs.orglett.9b04147.
[77] M.N. Aziz, A. Patel, A. Iskander, A. Chini, D. Gout, S.S. Mandal, C.J. Lovely, One-pot synthesis of novel 2-imino-5-arylidine-thiazolidine analogues and evaluation of their anti-proliferative activity against MCF7 breast cancer cell line, Molecules 27 (3) (2022) 841. http://doi: 10.3390/molecules27030841.
[78] T. Mosmann, Rapid colorimetric assay for cellular growth and survival: application to proliferation and cytotoxicity assays, J. Immunol. Methods 65 (1) (1983) 55–63, https://doi.org/10.1016/0022-1759(83)90303-4.
[79] C. Cui, Y. Chang, X. Zhang, S. Choi, H. Tran, K.V. Penmetsa, S. Viswanadha, L. Fu, Z. Pan, Targeting orai1-mediated store-operated calcium entry by RP4010 for anti-tumor activity in esophagus squamous cell carcinoma, Cancer Lett. 432 (March) (2018) 169–179, https://doi.org/10.1016/j.canlet.2018.06.006.
[80] S. Sreelatha, A. Jeyachitra, P.R. Padma, Antiproliferation and induction of apoptosis by moringa oleifera leaf extract on human cancer cells, Food Chem. Toxicol. 49 (6) (2011) 1270–1275, https://doi.org/10.1016/j.fct.2011.03.006.
[81] B.-Y. Choi, H.-Y. Kim, K.-H. Lee, Y.-H. Cho, G. Kong, Clofilium, a potassium channel blocker, induces apoptosis of human promyelocytic leukemia (HL-60) cells via bcl-2-insensitive activation of caspase-3, Cancer Lett. 147 (1) (1999) 85–93, https://doi.org/10.1016/S0304-3835(99)00280-3.
[82] Y. Liang, J. Chen, Q. Yu, T. Ji, B. Zhang, J. Xu, Y. Dai, Y. Xie, H. Lin, X. Liang, X. Cai, Phosphorylated ERK is a potential prognostic biomarker for sorafenib response in hepatocellular carcinoma, Cancer Med. 6 (12) (2017) 2787–2795, https://doi.org/10.1002/cam4.1228.
[83] M. Will, A.C.R. Qin, W. Toy, Z. Yao, V. Rodrik-Outmezguine, C. Schneider, X. Huang, P. Monian, X. Jiang, E. de Stanchina, J. Baselga, N. Liu,

S. Chandarlapaty, N. Rosen, Rapid induction of apoptosis by PI3K inhibitors is dependent upon their transient inhibition of RAS-ERK signaling, Cancer Discov. 4 (3) (2014) 334–347, https://doi.org/10.1158/2159-8290.CD-13-0611.

[84] T. Wang, M.-B. Wu, J.-P. Lin, L.-R. Yang, Quantitative structure–activity relationship: promising advances in drug discovery platforms, Expet Opin. Drug Discov. 10 (12) (2015) 1283–1300, https://doi.org/10.1517/17460441.2015.1083006.

[85] D.G. Sprous, R.K. Palmer, J.T. Swanson, M. Lawless, QSAR in the pharmaceutical research setting: QSAR models for broad, large problems, Curr. Top. Med. Chem. 10 (6) (2010) 619–637, https://doi.org/10.2174/156802610791111506.

[86] A.M. Aronov, C. Baker, G.W. Bemis, J. Cao, G. Chen, P.J. Ford, U.A. Germann, J. Green, M.R. Hale, M. Jacobs, J.W. Janetka, F. Maltais, G. Martinez-Botella, M. N. Namchuk, J. Straub, Q. Tang, X. Xie, Flipped out: structure-guided design of selective pyrazolylpyrrole ERK inhibitors, J. Med. Chem. 50 (6) (2007) 1280–1287, https://doi.org/10.1021/jm061381f.

[87] U.A. Germann, B.F. Furey, W. Markland, R.R. Hoover, A.M. Aronov, J.J. Roix, M. Hale, D.M. Boucher, D.A. Sorrell, G. Martinez-Botella, M. Fitzgibbon, P. Shapiro, M.J. Wick, R. Samadani, K. Meshaw, A. Groover, G. DeCrescenzo, M. Namchuk, C.M. Emery, S. Saha, D.J. Welsch, Targeting the MAPK signaling pathway in cancer: promising preclinical activity with the novel selective ERK1/2 inhibitor BVD-523 (ulixertinib), Mol. Cancer Therapeut. 16 (11) (2017) 2351–2363, https://doi.org/10.1158/1535-7163.MCT-17-0456.

[88] T.D. Heightman, V. Berdini, H. Braithwaite, I.M. Buck, M. Cassidy, J. Castro, A. Courtin, J.E.H. Day, C. East, L. Fazal, B. Graham, C.M. Griffiths-Jones, J. F. Lyons, V. Martins, S. Muench, J.M. Munck, D. Norton, M. O'Reilly, N. Palmer, P. Pathuri, M. Reader, D.C. Rees, S.J. Rich, C. Richardson, H. Saini, N.T. Thompson, N.G. Wallis, H. Walton, N.E. Wilsher, A.J.-A. Woolford, M. Cooke, D. Cousin, S. Onions, J. Shannon, J. Watts, C.W. Murray, Fragment-based discovery of a potent, orally bioavailable inhibitor that modulates the phosphorylation and catalytic activity of ERK1/2, J. Med. Chem. 61 (11) (2018) 4978–4992, https://doi.org/10.1021/acs.jmedchem.8b00421.

[89] C. Cui, Y. Chang, X. Zhang, S. Choi, H. Tran, K.V. Penmetsa, S. Viswanadha, L. Fu, Z. Pan, Targeting orai1-mediated store-operated calcium entry by RP4010 for anti-tumor activity in esophagus squamous cell carcinoma, Cancer Lett. 432 (2018) 169–179, https://doi.org/10.1016/j.canlet.2018.06.006.

[90] S. Choi, C. Cui, Y. Luo, S.-H. Kim, J. Ko, X. Huo, J. Ma, L.-W. Fu, R.F. Souza, I. Korichneva, Z. Pan, Selective inhibitory effects of zinc on cell proliferation in esophageal squamous cell carcinoma through Orai1, Faseb. J. 32 (2018) 401–416.